NTNU – Trondheim
Norwegian University of
Science and Technology

Design of Headworks in steep sediment loaded rivers

A model study case of Lower Manang
Marsyangdi Hydropower Project

Abha Dudhraj

Civil and Environmental Engineering
Submission date: June 2013
Supervisor: Leif Lia, IVM
Co-supervisor: Hanne Nøvik, IVM

Norwegian University of Science and Technology
Department of Hydraulic and Environmental Engineering

NTNU
Norges teknisk-naturvitenskapelige Universitet

Fakultet for ingeniørvitenskap og teknologi
Institutt for vann- og miljøteknikk

MASTER THESIS SPRING 2013

Student: ***Abha Dudhraj***

Title: **DESIGN OF HEADWORKS IN STEEP SEDIMENT LOADED RIVERS – A MODEL STUDY CASE OF LOWER MANANG MARSYANGDI Hydropower Project**

Tittel: UTFORMING AV INNTAK I BRATTE, SEDIMENTFØRENDE ELVER – MODELSTUDIE AV LOWER MANANG MARSYANGDI VANNKRAFTVERK

1 INTRODUCTION

A well-functioning intake is a prerequisite for the successful operation of a hydropower plant. The main challenges with developing good design principles for shallow intakes for hydropower plants involve sediment handling, floating debris, leaves, ice, entrainment of air and general hydraulic conditions. It is a major challenge to meet all these sometimes-incompatible requirements in the design of an intake in a shallow river with rapid flow. Internationally, and specifically in the Himalayas, with a heavy rainy season combined with a lot of sediments, sediment handling is the major concern. Settling basins are common components at headwork for minimizing sediment erosion of the waterways and the turbines. Therefore, a headwork design adapted to local conditions is essential. There are various principles for the design of intakes existing today;

some are more successful than others. Several intake structures undergo reconstruction or modification after only a few years in service, due to problems with maintenance and operation due to a design poorly adapted to local conditions.

Both private initiatives and hydropower companies are contributing with new solutions through model testing of headwork in the hydraulic laboratories. Hydro Lab Pvt. Ltd., Kathmandu and NTNU Vassdragslaboratoriet, Trondheim seeks to contribute to further development, verification and innovation within this area.

2 BACKGROUND

Sediment handling in steep sediment loaded rivers normally requires settling basins. Flushing of settling basins and sand traps is widely used, and different flushing concepts have been developed. Because of the unique conditions for every single hydropower project and the complexity of the sediment transport, physical and/or numerical model studies of the headwork are often recommended. Experiences from existing hydropower plants and available physical models are very valuable tools for planning and design of new headwork. A physical model of the headwork of the 138 MW Lower Manang Marsyangdi Hydropower Project (LMM HPP), located in Manang District of Gandaki Zone in Nepal, is built at Hydro Lab Pvt. Ltd. in Kathmandu, Nepal. The plant is scheduled to be commenced by 2017.

3 PROBLEM DESCRIPTION

Theory of headwork design in general, and sediment handling especially, in addition to experiences from case studies from hydro power plants already built must be studied. A test program shall be designed for a model study of the headwork of the LMM HPP. The goal of the physical model study of the LMM HPP conducted at Hydro Lab Pvt. Ltd. is to evaluate the given design and improve the performance of the headwork especially with respect to sediment handling arrangement, both during normal conditions and during floods. Modified intake arrangement should be tested for normal monsoon flow and flows higher than this. The tests should include study of flow patterns in the intake area and the settling basins; bed control in front of the intake and passage of floating debris. Specific aspects of the headwork hydraulics should

be assessed by a numerical model study, and compared to observations from the physical model. All the tests should be documented and reported.

4 GOAL

The overall goal of the master thesis is to gain experiences on intake hydraulics and headwork design. Theoretical aspects of headwork design must be implemented during the assessment of the performance of the LMM headwork. Uncertainties and errors should be evaluated. It should be concluded on whether the work has been successful or if there should be further studies needed to be conducted.

5 CONTACT PERSONS

NTNU	Leif Lia, Professor (supervisor)
	Hanne Nøvik, PhD-student (co-supervisor)
Hydro Lab Ltd	Durga P. Sangroula
	Usha Shrestra
Butwal Power Company (BPC)	Pratik Man Sing Pradhan

Discussions with colleagues and employees at NTNU, SINTEF, Hydro Lab, BPC and eventually other hydro power plants are recommended. All contributions should be correctly referred.

6 REPORT FORMAT, REFERENCES AND CONTRACT

The report should be written with a text editing software, and figures, tables, photos etc should be of good quality. The report should contain an executive summary, a table of content, a list of figures and tables, a list of references and information about other relevant sources. The report should be submitted electronically in B5-format .pdf-file in DAIM, and three paper copies should be handed in to the institute.

The executive summary should not exceed 450 words, and should be suitable for electronic reporting.

The Master's thesis should be submitted within Monday 10th of June 2013.

Abstract

Headworks design in steep, sediment loaded rivers is challenging. Technical challenges related to the functionalities of the headworks area have been studied for the case of Lower Manang Marsyangdi (LMM) Hydropower Project (HPP), which is under design phase in Nepal. The Physical Hydraulic Model (PHM) study conducted at Hydro Lab focuses on intake hydraulics, sediment handling and trash removal along the intake. Experience from the physical model study of the LMM headworks has shown that the passage of sediments and bed control during flood periods are the major challenges in this hydropower project. Design of an optimal bed load handling component and the settling basin are very important to handle sediments without affecting the regularity in power generation.

Velocity measurements were conducted at several cross-sections along the settling basins to evaluate the hydraulics. Turbulent Kinetic Energy (TKE) was calculated from the velocity measurements to assess the effect of secondary currents. The study has further focused on the concept of numerical modeling to replicate the hydraulics in the existing headworks model of LMM HPP. A Three-dimensional (3D) CFD-program, STAR CCM+, has been used to conduct the numerical model study of the intake hydraulics of LMM headworks.

Through dye tests and measurements on the PHM it has been shown that final conceptual design, which is based on modifications conducted on the initial design, has an improved hydraulics along the intake. Vortices/eddies in front of the intakes and along the settling basins have been reduced and a uniform, symmetrical flow with the desired velocity of less than 1.00 m/s prototype value has been achieved along the settling basins. Further evaluation of TKE has shown significant decrease of turbulence level along the settling basins.

Use of numerical model has to a large extent been successfully able to replicate the hydraulics in the modeled headworks of LMM HPP. The velocity range is comparable to the measured values in the laboratory. However, secondary currents and, thereby, the TKE values have not been reproduced properly in the numerical model. TKE for the first cross-section close to the inlet of the basin is

similar but no significant trend can be observed between the other cross-sections.

Numerical model requires boundary conditions determined from the PHM and results need to be validated against laboratory measurements to ensure their accuracy. Thus, it is recommended for numerical model studies to be used in combinations with PHM study. Numerical model requires an initial validation by comparing simulated flows to measured flows from the laboratory. The validated numerical model can then be used to predict further effects of modification in the headworks design and to optimize the conceptual design.

Sammendrag

Basert på resultatene fra det fysiske modellstudiet har det blitt konkludert med at utforming av inntak i bratte, sedimentførende elver er spesielt utfordrende.Tekniske utfordringer knyttet til inntaksområdet har blitt vurdert for Lower Manang Marsyangdi (LMM) vannkraft prosjekt i Nepal. Inntakhydraulikken i tillegg til håndtering av sediment og drivgods langs inntaket har blitt fokusert på i det fysiske modellstuidet gjennomført i samarbeid med Hydro Lab.

Hastighetsmålinger ble utført langs flere tverrsnitt langs sedimenteringsbassengene i den fysiske modellen for å evaluere strømningsforholdene. Turbulent Kinetisk Energi (TKE) ble beregnet fra hastighetsmålinger for å vurdere effekten av sekundære strømninger i bassengene. Videre er det brukt numerisk modellering for å gjenskape hydraulikken langs inntaksområdet i den fysiske modellen av LMM. Den tredimensjonale (3D) CFD-program, STAR CCM +, har blitt brukt til å utføre denne simuleringen.

Forbislipping av sedimenter og kontroll av bunnivå ved inntaket, spesielt for flomperioder, er de største utfordringene i dette vannkraftsprosjektet. Utformingen av en velfungerende bunnspyleluke og sedimenteringsbassenget er svært viktig for å kunne håndtere sedimenter uten å ha for store innvirkninger på kraftverksproduksjonen.

Ved bruk av markørvæske har det blitt utført tester og målinger i den fysiske modellen. Den endelige utformingen av inntaksområdet, som er basert på modifikasjoner av den opprinnelige utformingen, har en klar forbedret hydraulikk langs inntaket. Virveldannelser foran inntaksåpningene og langs sedmenteringsbassengene er redusert, og en jevn og symmetrisk strømning med hastighet på mindre enn 1.00 m/s i prototyp verdi, er oppnådd langs bassengene. Videre evaluering av TKE har vist betydelig reduksjon av turbulensnivå langs med sedimenterings bassengene.

Bruk av den numeriske modellen har i stor grad vært vellykket og er i stand til å gjenskape inntakshydraulikken i den fysiske modellen av LMM. Hastighetene er

sammenlignbare med de målte verdiene i laboratoriet. Derimot, har ikke den numeriske modellen klart å gjenskape sekundære strømningene og TKE verdier fra den fysiske modellen. TKE for det første tverrsnittet som er i nærheten av innløpet til sedimenteringsbassengene samsvarer bra med de målte verdiene, men for de andre tversnittene derimot, er det ingen tydelig samsvar mellom de målte og simulerte verdiene.

Numeriske modeller krever grensebetingelser som kan bestemmes fra målte verdier fra fysiske modeller og resultatene må vurderes opp mot laboratoriemålinger for å verifisere nøyaktighet i resultatene fra simuleringene. Således er det anbefalt å bruke et numeriske modellstudie i kombinasjon med et fysisk modellstudie. Resultatene fra numeriske modeller må kontrolleres ved å sammenligne de mot målte verdier fra laboratoriet/felt. Deretter kan den numeriske modellen brukes for å forutsi ytterligere effekter ved endringer i utforming av ulike inntakskomponenter og for å optimalisere modellen frem til den endelige design.

Preface

This report is developed as an output of the Master's thesis conducted under the guidance and co-operation of the Institute of Hydraulics and Environmental Engineering.

The thesis is a combination of a Physical Hydraulic Model study and a Numerical Hydraulic Model study conducted on the headworks of Lower Manang Marsyangdi Hydropower project under design in Nepal.

The study has increased my understanding on intake hydraulics and sediment-related problems in hydropower plants with steep, sediment-loaded rivers. The thesis has also given me the opportunity to learn a new software program, Star CCM+, its applications and the use of numerical model as a tool in the verification and understanding of river hydraulics.

I would first and foremost, like to extend my gratitude to my supervisor Leif Lia for the necessary support provided for the development of this thesis. Furthermore, I would like to sincerely thank my co-supervisor Hanne Nøvik who has constantly encouraged me and provided continuous supervision to aid the writing of this thesis. Guidance from Torgeir Jensen, SINTEF, on the usage of ADV measurements in the laboratory is deeply appreciated. Similarly, the suggestions and assistance provided by the staff at Hydro Lab Pvt. Ltd. during my stay in Nepal is immensely valued. Last but not the least; I am very grateful to my friends and family for the adequate moral support during this period.

Table of Contents

1 Introduction 1

2 Background 3

2.1 The Lower Manang Marsyangdi HPP 3

2.2 Challenges in LMM HPP 5

3 Theoretical background 9

3.1 Design of headworks in steep sediment loaded rivers 9

3.1.1 Performance standards 10

3.1.2 Intake hydraulics 13

3.1.3 Settling Basin Design 15

3.2 Model theory 18

3.3 Numerical Modeling – CFD 20

3.3.1 Grids 20

3.3.2 Navier Stokes equations 20

3.3.3 Discretization methods 21

3.3.4 Turbulence models 22

3.3.5 Stability and convergence 23

3.3.6 Courant Number 24

4 Methodology 25

5 Physical hydraulic model study of the headworks of LMM HPP 27

5.1 Model study methodology 27

5.2 The initial design 28

5.3 Analysis of the initial design against the Final arrangement 30

5.3.1 Intake Hydraulics 30

6 Velocity measurements on the Physical Hydraulic Model of LMM HPP 39

6.1.1 Acoustic Dopple Velocity Meter (ADV) 39

6.2 Procedure for the ADV measurements 40

6.3 Micro propeller measurements 42
7 Numerical model study of the headworks of LMM HPP 45
7.1 Star CCM+ 45
7.2 The numerical model setup 45
7.2.1 Pre-processing 45
7.2.2 Post processing 55
8 Results 57
8.1 Results from the numerical simulation 57
8.1.1 Reliability and convergence of the numerical simulation 57
8.1.2 Streamlines 58
8.1.3 Pressure 59
8.1.4 Velocity distribution 60
8.1.5 Turbulent kinetic energy (TKE) 60
8.1.6 Vorticity 61
8.2 Results from measurements in the physical model 61
8.2.1 Velocity measurements along the intake 61
8.2.2 Velocity measurements along the gravel trap 62
8.2.3 Comparison of measurements and simulations 63
8.3 Vorticity in the numerical simulation 70
9 Discussion 73
9.1 Physical Hydraulic Model studies of Headworks 73
9.2 Measurements on the Physical Hydraulic Model 75
9.3 Comparison of simulated results and measurements 76
10 Conclusion 79
11 Further work and Recommendations 81
Bibliography 83
Appendix A Case studies of headworks design of physical hydraulic models (PHM) 85

Kabeli A HPP 85
Initial arrangement vs the Final arrangement..... 86
Khudi HPP 93
The initial arrangement..... 94
Modifications adopted for the final arrangement 95
Effects and Evaluation of the modifications..... 98
Appendix B Salient features for the initial headworks design of LMM HPP 101
Appendix C Velocity distributions along various Cross-Sections (CS) 103
12 Appendix D Plan layout of the final design of LMM..... 105

List of figures

Figure 1 Location of LMM (source: googlemaps) 3
Figure 2 Initial PHM LMM (Shrestha and Bogati, 2012) 4
Figure 3 Upstream river conditions of the headworks site of LMM (Nielsen and Rettedal, 2012) 5
Figure 4 Sediment transportation rates LMM (Shrestha and Bogati, 2012) 6
Figure 5 Flow Duration Curve LMM HPP (Shrestha and Bogati, 2012) 7
Figure 6 PSD for flow up to Average Monsoon Flow LMM HPP (Shrestha and Bogati, 2012) 7
Figure 7 Major headworks components (Jennsen et al., 2006) 9
Figure 8 Turbulent flow fields near the intake(Jennsen et al., 2006) 10
Figure 9 Spillway at Middle Marsyangdi HPP 11
Figure 10 Intake cloggage at Khudi HPP(Shrestha et al., 2008) 12
Figure 11 Undersluice slots at Middle Marsyangdi HPP (Nielsen and Rettedal, 2012) 12
Figure 12 Turbulent flow regimes (Oslen, 2011) 14
Figure 13 Sediment deposition in the settling basins of Khudi HPP 15
Figure 14 General layout of settling basin (Lysne et al., 2003) 17
Figure 15 Flow tranquilizers at the inlet of 17
Figure 16 Different type of grid structures (Hasaas, 2012) 20
Figure 17 Comparison of the model and prototype of the headworks site of LMM HPP (Shrestha and Bogati, 2012) 28
Figure 18 Initial physical model of the headworks of LMM HPP (Shrestha and Bogati, 2012) 29
Figure 19 Final arrangement of the intake of the PHM of LMM HEP 30
Figure 20 Problems downstream on the inital arrangenement of the PHM of LMM HPP (Shrestha and Bogati, 2012) 31
Figure 21 Initial design of the bed load hopper 32
Figure 22 Bed control at the initial arrangement of LMM HPP (Shrestha and Bogati, 2012) 33
Figure 24 Settling basin inlet in the initial arrangement of LMM HPP (Shrestha and Bogati, 2012) 34
Figure 23 Bed Control at the final arrangement of LMM HPP 34
Figure 25 Settling basin outlet in the initial arrangement of LMM HPP 35
Figure 26 Final arrangement of the SB of LMM HPP 35

Figure 27 Final arrangement of the approach canals in the PHM of LMM HPP 36
Figure 28 Final arrangement on theSettling Basin outlet in the PHM of LMM HPP 36
Figure 29 Final arrangement of the PHM of LMM HPP..... 37
Figure 30 Standard ADV Field Probe 39
Figure 31 Side looking 3D probe 40
Figure 32 ADV measurements along the settling basins of the PHM of LMM HPP 40
Figure 33 Measured Cross-sections along the Settling Basins of LMM HPP..... 41
Figure 34 ADV measurements at the intake orifice of LMM HPP 42
Figure 35 Mini Air 20 Micropropeller..... 42
Figure 36 MicroPropeller measurements at the intake of the PHM of LMM HPP 43
Figure 37 Imported geometry from AutoCAD; x-direction shows the direction of flow..... 46
Figure 38 Surface parts in the NHM 47
Figure 39 Surface diagnostics of the NHM 47
Figure 40 Volume mesh at the intake 49
Figure 41 Derived parts in the NHM..... 53
Figure 42 Residual plot of the numerical simulation 57
Figure 43 Mass flow plot of the numerical model 58
Figure 44 Streamlines of the numerical model 59
Figure 45 Pressure development in the numerical model 59
Figure 46 Velocity distributions along a plane section in the numerical model 60
Figure 48 Vorticity along the settling basin..... 61
Figure 47 Distribution of turbulent kinetic energy in the model 61
Figure 49 Velocity measurements along the intake..... 62
Figure 50 Velocity measurements along the gravel trap 63
Figure 51 Comparison of velocity field close to the bottom of the settling basin 64
Figure 52 Comparison of velocity field along the middle plane section of the settling basin 64
Figure 53 Comparison of velocity field close to the surface of the settling basin 64
Figure 54 Velocity field settling basin LMM ,Cross-section 2..... 66
Figure 55 Comparison of TKE development along the settling basin 67

Figure 56 TKE along the settling basin 68
Figure 57 TKE at Cross-section 4 68
Figure 58 Velocity along the gravel trap 69
Figure 59 TKE based on ADV measurements along the gravel trap..... 69
Figure 60 Simulation of vorticity along the settling basin..... 70
Figure 61 Simulated vorticity at various depths..... 71
Figure 62 Headworks site of Kabeli'A' HPP(Bogati, 2012)..... 85
Figure 63 Kabeli A Headworks of the initial design (Bogati, 2012) 86
Figure 64 Initial (Left) vs Final (right) intake design Kabeli 'A' 87
Figure 65 Initial design of the stilling Basin at Kabeli'A' HPP(Bogati, 2012)..... 88
Figure 66 Final design of the stilling basin at Kabeli 'A' HPP 88
Figure 67 Final design of the approach tunnels for the PHM of kabeli 'A' HPP 91
Figure 68 Final design settling basin Kabeli 'A' HPP 91
Figure 69 Modifications at the approach tunnel and inlet transition of the settling basin(Bogati, 2012)..... 92
Figure 70 Final arrangement Kabeli 'A' HPP 92
Figure 71 Headworks site of Khudi HPP (Shrestha et al., 2008)..... 93
Figure 72 PHM of the headworks of Khud HPP (Shrestha et al., 2008) 94
Figure 73 Modifications at the intake of PHM of Khudi HPP (Shrestha et al., 2008)..... 96
Figure 74 Modifications along the gravel trap on the PHM of Khudi HPP (Shrestha et al., 2008) 97
Figure 75 Modifications at the downstream river slope of Khudi HPP (Shrestha et al., 2008)..... 97
Figure 76 River training structures Khudi model (Shrestha et al., 2008) 97
Figure 77 River training structures at the intake of PHM of Khudi HPP (Shrestha et al., 2008)..... 98
Figure 78 Final arrangement of the PHM of Khudi HPP 98

List of tables

Table 1 Flow discharge LMM (Shrestha and Bogati, 2012) 6
Table 2 Classification of the flushing systems 13
Table 3 Scale ratios for various parameters when using the Froude model law (Lysne, 1982) 19
Table 4 Measured Cross-sections along the Settling Basins of LMM HPP 41
Table 5 Overview of the selected mesh models 48
Table 6 Overview on the selected physics model 51
Table 7 Selected boundary conditions 54
Table 8 Under-relaxation factors used in the numerical model 55

List of Symbols

Symbol	Definition
LMM	Lower Manang Marsyangdi
HPP	Hydropower Project
ROR	Run-of-River scheme
CFD	Computational fluid mechanics
BPC	Butwal Power Company
DoED	Department of Electricity Development
m/s	Metre per second
m^3/s	Cubic metre per second
Mm^3	Million cubic metre
SB	Settling Basin
CS	Cross-section
ADV	Acoustic Doppler Velocimeter
3-D	Three dimensional
S4	Serpent Sediment Sluicing System
DNS	Direct Numerical simulation
LES	Large Eddy Simulation
RANS	Reynolds Averaged Navier Stokes Equations
TKE/k	Turbulent kinetic energy
δ_{ij}	Kronecker delta
v_T	Eddy viscosity
ω	Specific dissipation rate
ε	Dissipation of Turbulent kinetic energy
STL	Stereo Lithography
VOF	Volume of fluid
Fr	Froude number
Q	Discharge
t	Time
MW	Mega Watt
GWh	Giga Watt hour
m	metre
Re	Reynolds number
D	Diameter
L	Length
u	velocity
v	Kinematic viscosity
ρ	Density
masl	metre above sea level

1 Introduction

Steep rivers mounting from the glaciers in the Himalayas along with varying topography and heavy monsoon periods provide Nepal with a huge potential for hydropower development. Consequently, with nearly 86% of the electricity supply from hydropower (Nai, 2004) Nepal is heavily reliant on water resources. The total estimated hydropower potential is 83 000MW out of which 43 000MW is deemed technically and economically viable for development. However, due to the social and economical complications in the country the total installed capacity amounts to 705 MW (Shrestha, 2012). Furthermore, according to a world bank study about 63% of the Nepalese households lack access to electricity (Banerjee et al., 2011). The deficiency in electricity is therefore creating an enormous need for development in the hydropower sector in the years ahead.

A functional intake is a prerequisite to ensure successful operation of both the existing and new Hydropower Projects (HPP) that are under development. Proper conceptual planning and design of the headworks is therefore required for the further development of HPP in the country. Technical challenges related to the headworks area have been studied for the case of Lower Manang Marsyangdi (LMM) HPP in further detail in the following chapters. Intake hydraulics along with sediment handling and trash removal has especially been focused.

Lower Manang Marsyangdi Hydropower Project (LMM HPP) located in the Gandaki zone in western Nepal has been studied and designed for development by Hydro Consult Engineering Limited (Ltd.) for Butwal Power Company (BPC). Physical model study of the headworks area is being conducted at Hydro Lab Private Limited (Pvt. Ltd.), hydraulic laboratory in Nepal in order to assess the overall performance of the headworks design in terms of its functionality.

A field trip to Nepal was conducted during the course of this thesis in order to use existing theories and experiences from previous physical model studies conducted in Hydro Lab to evaluate the intake hydraulics and headwork design of LMM HPP. In order to gain experience from previous physical model studies two case studies have been conducted based on reports prepared by Hydro Lab during the two months stay in Nepal. The first case study presented is the

performance assessment of the headworks of Kabeli 'A' HPP designed and studied for development. The second case is the study of existing headworks of Khudi HPP, which had been suffering from intake clogging already during the plants first year of operation. The two case studies mentioned are presented in Appendix A.

The design of LMM HPP as provided by Hydro Consult has been evaluated and compared with the design improvements suggested by Hydro Lab for the final design. Flow patterns and headworks performance have been studied at the intake and along the settling basin. Velocity measurements were conducted at several cross-sections to evaluate the hydraulics along the settling basins. Turbulent Kinetic Energy (TKE) values have also been calculated from velocity measurements to assess turbulence in the basins and develop turbulence level as a design criteria for settling basins.

The study has further focused on the concept of numerical modeling to replicate the hydraulics in the existing headworks model of LMM HPP. The three dimensional (3D) CFD-program, STAR CCM+, is used to conduct a numerical model study of the intake hydraulics of LMM HPP. The results from the numerical model are compared to the measurements from the model studies, conducted at Hydro Lab. The comparison is used to assess the errors and reliability of the numerical model study and to determine whether numerical models are useful in predicting hydraulic problems at the intake.

2 Background

2.1 The Lower Manang Marsyangdi HPP

Butwal Power Company (BPC) established and operating in Nepal has obtained the survey license to develop LMM HPP from the Department of Electricity Development (DoED), Government of Nepal. The feasibility study is completed and the detail design phase is near completion. The construction is planned to be commenced by 2017 (BPC, 2011).

LMM HPP is located in the southern part of Manang district in Gandaki zone of Western Nepal shown by Figure 1. The headworks site lies in Bagarchhap with a catchment area of 1694 km^2 and the Powerhouse site at Khotro. The drop from Tachai-Bagarchhap to Dharapani of the Marsyangdi River is utilized for power production. The gross head is estimated to be approximately 320m.

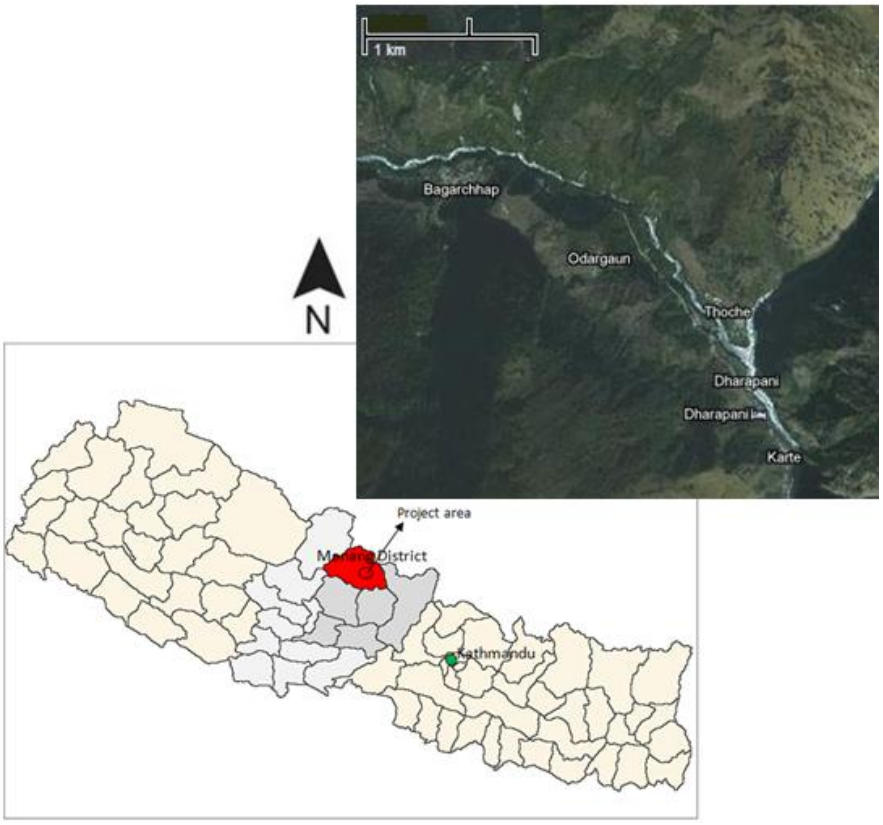

Figure 1 Location of LMM (source: googlemaps)

With a design discharge of 52.0 m^3/s during the wet season this run-of-river scheme (ROR) HPP is designed for an installation capacity of 138MW and an average annual estimated general energy production of 735 GWh.

The initial design of the plant is based on the concept of side intake with two intakes each with two openings. The weir is a concrete gravity dam of 45m in length designed with two undersluice radial gates and required spillway capacity followed by a stilling basin. A gravel trap with flushing arrangements follows each of the intakes further into a pressure chamber, which leads into a settling basin consisting of a double basin, divided into two minor ones. A physical hydraulic model (PHM) developed in a scale ratio of 1:40 is shown in Figure 2 based on the initial design as provided by the client to Hydro Lab. Further details of the salient features can be viewed in Appendix B.

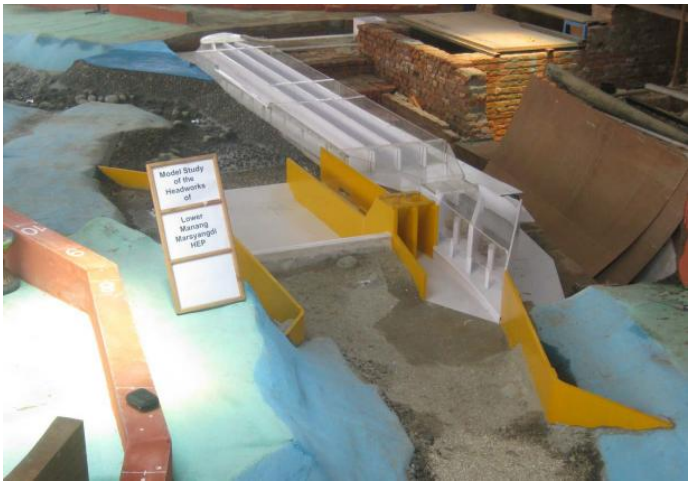

Figure 2 Initial PHM LMM (Shrestha and Bogati, 2012)

2.2 Challenges in LMM HPP

Rivers in Nepal are among the rivers with the highest sediment yield in the world exceeding 10 000 tonnes/km^2/year in some of the rivers such as Kulekhani (Shrestha, 2012) caused by the climatic, tectonic and geological factors. The seasonal load variation with high intensity of rainfall for a short period during the rainy season, also known as monsoon, causes a large number of landslides adding sediments to the river systems. Similarly, the rapid uplifting of the mountains has caused fracturing and weathering of the rock masses increasing the amount of sediments available. In addition to this, the mountainous rivers of Nepal are very steep, and the general gradient is 32 m/km. As such the transport and erosive capacity of these rivers is tremendous, this is further enhanced by the small cross-sections due to gorges.

Conditions mentioned above are also prevalent along the project site of LMM. Thus, there are several challenges related to the project's design and optimization. The sediment yield at the Marsyangdi river is estimated to be approximately 7700 tonnes/km^2/year(Shrestha, 2012). The upstream part of the river runs through deep ravines and steep valleys as can be seen from Figure 3. During the monsoon season with occurrences of large-scale landslides in steep areas the river is heavily loaded with sediment and considerable amount of sediments is expected to be transported along the river.

Figure 3 Upstream river conditions of the headworks site of LMM (Nielsen and Rettedal, 2012)

Suspended sediment sampling of the Marsyangdi River has been conducted at the vicinity of the headworks by the Client from 2009 till date. Based on the measured suspended sediment discharges conducted by the Client the amount of total suspended discharge is estimated to be approximately 59.0 kg/s at the headworks site during the river flow equivalent to design discharge with 20% additional discharge for flushing at the intake. The suspended sediment discharge increases to 180.0 kg/s during the Average Monsoon Flow period.

From Figure 4 below we can see the sedimentation rates as adopted by Hydro Lab for the physical hydraulic model studies at various discharges. The increase in transport rate of the suspended sediment is significantly larger during high discharges and flood due to the increase in turbulence in the water.

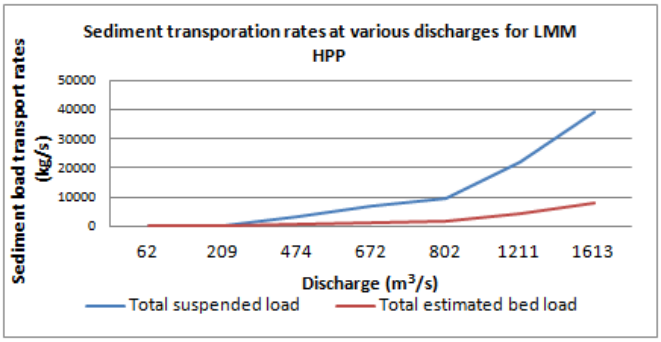

Figure 4 Sediment transportation rates LMM (Shrestha and Bogati, 2012)

Table 1 Flow discharge LMM (Shrestha and Bogati, 2012)

Return Period	Flow (m^3/s)
Design Discharge	52.0
Average annual flow	46.0
Average Monsoon flow	109.0
Average Monsoon Flood	287.0
10 Year Flood	802.0
100 Year Flood	1211.0
1000 Year Flood	1613.0

In addition to this, steep river conditions along with high discharges during the monsoon period, as shown in Table 1, provides the river with high sediment transportation capacity. According to the physical model study, boulders up to 0.90 m were found to be transported along the river stretch during a 5-year flood. Here, the gradient of river governs the amount of sediment transported rather the sediment capacity of the river itself.

The design discharge, 52.0 m^3/s, is only available 33% of the time as shown from the Flow duration curve in Figure 5 consequently problems related to flushing arrangements may arise during operation and the designed power generation is only possible three months during the monsoon period.

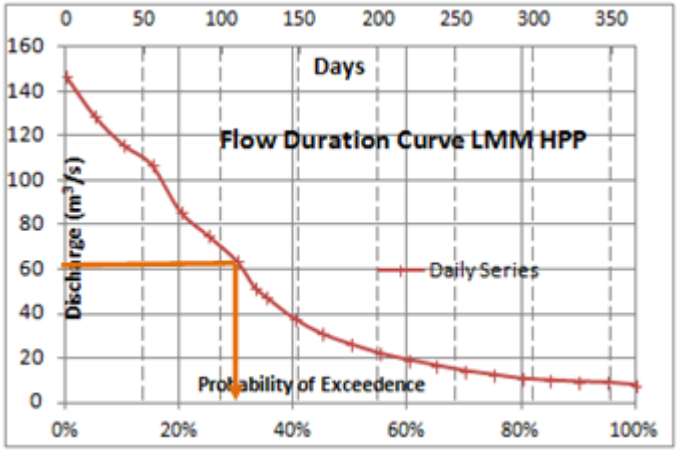

Figure 5 Flow Duration Curve LMM HPP (Shrestha and Bogati, 2012)

In addition to this, almost 80 % of the sediment particles are noted to be sand particles with a diameter size of less than 2.00 mm. A particle size distribution (PSD) curve for flows up to the average monsoon flow as prepared by Hydro Lab is shown in Figure 6. Sediment handling at the intake and along the settling basins therefore needs to be well taken care in order to minimize wear and tear of the mechanical components in the system.

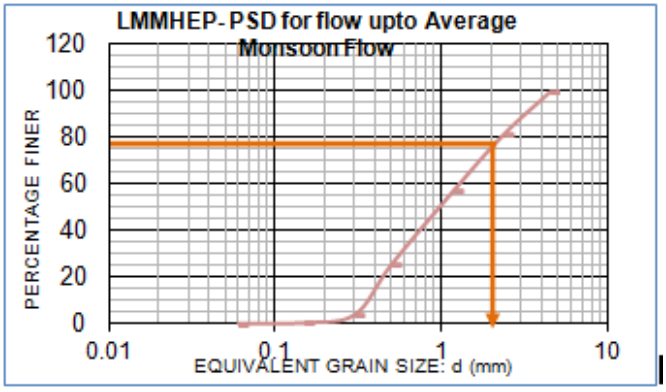

Figure 6 PSD for flow up to Average Monsoon Flow LMM HPP (Shrestha and Bogati, 2012)

According to the test observations of the base case in the physical model, which is the initial design of the project as provided by the client, the intake did not appear to function optimally. Several problems were observed at the intake. The design was incapable of maintaining bed control in front of the intake; bed load sluices lacked sufficient suction capacity, which eventually led to the clogging of intake. Similarly, turbulent flows near the intake led to uneven flow distribution to and along the settling basins. Design with respect to hydraulic performance of the headworks and its sustainability is reviewed and discussed in further detail in Chapter 5.

3 Theoretical background

The following sections provide a theoretical background for the topics that are dealt with in this thesis. Factors that affect the design of headworks in steep sediment loaded rivers are discussed in chapter 3.1. Parameters related to intake hydraulics and design of settling basin has been presented in further detail under sections 3.1.2 and 3.1.3 respectively. Chapter 3.2 gives an understanding of the model theory behind Physical hydraulic models. Furthermore, the topic of numerical modeling is presented in chapter 3.3.

3.1 Design of headworks in steep sediment loaded rivers

One of the major challenges in a hydropower project is successful diversion of water out of the river. Headworks, also referred to as diversion works, abstracts the water from the river and diverts it into the waterways of the HPP for power generation at various flow conditions and assists safe discharge of flood. As such, the headwork consists of all structural components required for water diversion, energy dissipation, handling of sediments, and floating debris. Figure 7 gives an overview of the major headwork components.

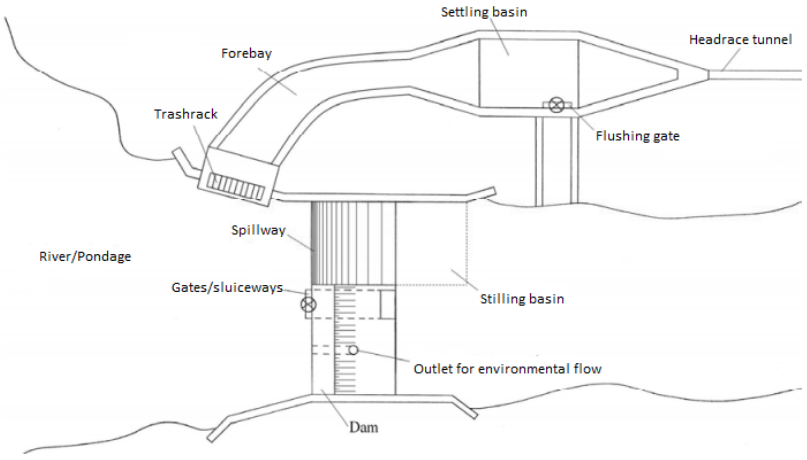

Figure 7 Major headworks components (Jennsen et al., 2006)

The design of the various headworks components will vary depending on site-specific conditions, such as topography, geology, hydrology, meteorology, sedimentology and environment, and needs to be adjusted accordingly. Every HPP has a unique headworks arrangement. Consequently, the selection of

headworks site should be based on the location's technical, economic and environmental suitability for the major components that form the headworks.

3.1.1 Performance standards

Poor performances of headworks causes reduced efficiency in the production from the plant and leads to substantial economic losses. In order to address concerns related to headworks design in a systematic way performance standards developed by Lysne et al. (2003) have been discussed below.

Withdrawal of water

Headworks of a ROR plant needs to be capable of abstracting the amount of water required for power generation and bypassing the surplus. The HPP have to be designed such that the plants are able to extract design discharge from the river even during dry season. Diversion weir (dam) along with the intake diverts and controls the abstraction of water into the conveyance system.

A submergence of the intake is required so that the water level in the river is high enough for necessary abstraction of flow even during dry seasons and for the prevention of air entrainment in the conveyance system. River training works are used to provide favorable curvature of flow near the intake. Guide walls are usually constructed to constrain the flow in front of the intake. The shape of the guide wall and the alignment of the intake should be designed to ensure a uniform flow at the inlet of the intake. Turbulence is reduced due to the smooth accelerating flow towards the intake. Figure 8 shows intake designs that are undesirable and can create turbulent flow fields near the inlet.

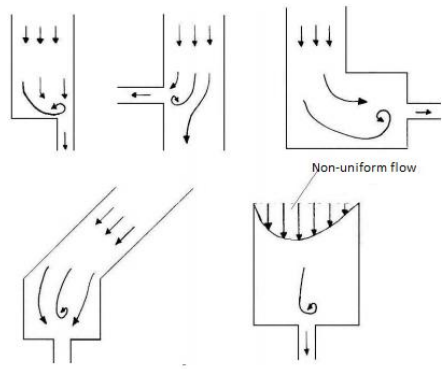

Figure 8 Turbulent flow fields near the intake(Jennsen et al., 2006)

Passage of floods, including hazard floods

The headworks structure needs to be designed to facilitate a safe passage of the design flood without causing serious damages to the headworks. A flexible headworks arrangement is required in the Nepalese rivers due to limited flow records and uncertainties in the estimates. Flash floods due to natural hazards

such as the Glacier lake outburst flood (GLOF) or overtopping should be handled with some structural damages.

Spillways, as shown in Figure 9, allow excess flood to pass safely over the diversion structure. Similarly, gated outlets are used to control discharges made to the river downstream. Energy dissipation structures (stilling basin) is placed downstream of the diversion structure such that the river past the spillway does not cause serious scouring or damage. In addition to this, supplementary structures, such as the bypass spillway, upstream- and downstream divide wall, guide the flow and prevent scouring and hydraulic jumps.

Figure 9 Spillway at Middle Marsyangdi HPP

Passage of ice, trash and floating debris

Accumulation of the debris in front of the intake causes significant changes in the flow pattern near the intake. Increase in turbulence level and head loss across the intake are some of the resulting consequences. Thus, the design needs to allow the passage of all ice, trash and floating debris with the use of debris gates and trash racks.

Trash racks in front of the intake, as shown in Figure 10, prevent the passage of undesired materials through the intake. The velocity across the inlet should be maintained in order to be able to clean the trash rack manually. Hydraulic losses over the trash rack also needs to be considered, which is a function of the water velocity and the geometry of the trash rack (Jennsen et al., 2006).

Passage of sediments

Nepalese rivers are highly sediment loaded and the design of the headworks must prevent the bed-load from approaching the intake and causing clogging of the intake like in Figure 10. The design needs to facilitate the passage of bed-load through sluiceways without causing significant structural damages to the headworks components.

The run-of-river schemes in sediment-loaded rivers need to be designed such that most of the sediment is transported along the river flow that is remaining after abstraction of water into the waterways. The transportation of sediment with the river flow can be obtained by two ways (Guttormsen, 2006) :

- Separation of the sediments before the intake
- Flushing of sediments from the intake structure

Figure 10 Intake cloggage at Khudi HPP(Shrestha et al., 2008)

The inlet of the intake needs to be placed above the intake bed such that the bed load and sediments in the lower layer of the flow are separated from upstream the intake at all flow conditions.

Bed control at the intake

In order to avoid the riverbed from building up at the intake and causing clogging and uneven flow distribution, the intake either needs to be located close to the spillway gates or should be equipped with under-sluices, as shown in Figure 11.

Figure 11 Undersluice slots at Middle Marsyangdi HPP (Nielsen and Rettedal, 2012)

Exclusion of suspended sediments and air

Suspended sediments need to be removed from the diverted water with the use of settling basins to avoid sediment problems in the waterways and the hydraulic machineries. The design of settling basin, which is a key concept for sediment exclusion in plants has been discussed in detail in section 3.1.4. In order to avoid air entrainment problems in the conveyance system air vents need to be designed.

Flushing of settled sediments

Efficient flushing of the sediments from the settling basins needs to be ensured such that its capacity remains unaltered. The removal of sediment from the

basins is usually done by flushing with the use of flushing gates. A dead storage is, however, provided where sediments are accumulated between two consecutive flushing, which further depends on the sediment load and the flushing method.

Other flushing systems that have been developed are the S4 (Serpent Sediment Sluicing System) by Professor Dr. Haakon Støle described in Støle (1993) and the sedicon sluicer (The slotted pipe sediment Sluicer) by Professor Dr. Tom Jacobsen presented in Jacobsen (1997). Flushing operations need to be preferably designed such that the power generation capacity of the plant is least affected. Some methods may require HPP closure during flushing, whereas others allow a continuous operation during flushing. The flushing systems can be classified according to Table 2 (Lysne et al., 2003):

Table 2 Classification of the flushing systems

SETTLING BASIN FLUSHING ARRANGEMENT			
Close down during flushing		**In operation during flushing**	
1 Conventional gravity flow flushing	2 Excavators and manual unloading	3 Continuous flushing	4 Intermittent flushing

3.1.2 Intake hydraulics

The flow distribution, turbulence level and eddy formations in these steep and sediment-loaded river dominates the river hydraulics, which in return influences the intake hydraulics. The river in motion and the interactions between the river and its surrounding environment therefore needs to be investigated in order to develop functional design structures and avoid frequent maintenances (Chanson, 2004).

Turbulence

Based on the impact of viscosity in fluid the flows can be classified accordingly. Laminar flows with low velocities, where the effect of viscosity is dominant has water particles traveling in smooth relatively straight lines without mixing. With increasing velocity the inertial forces overshadow the viscous effects in the fluid and the particles move in an irregular path causing momentum exchange between two portions of the fluid, thereby, causing eddy formations. The cascade of eddies is called turbulence, where the smaller eddies are given

energy by the largest eddies and the main flow provides energy to sustain the lager eddies.

Which of these flows are dominant in a channel is dependent on the Reynolds number, Re, which, is dependent on the velocity, u, characteristic length, L and kinematic viscosity, ν .

$$Re = \frac{u*L}{\nu} \tag{3.1}$$

In open channels such as a river, the flow is considered turbulent for a Reynolds number above 12500. Figure 12 exhibits a typical point velocity measurement in a turbulent flow regime with a steady mean value U and a fluctuating component u'(t). A turbulent flow is here characterized by the mean value of its velocities and a statistical property of their fluctuations (Versteeg and Malalasekera, 2007).

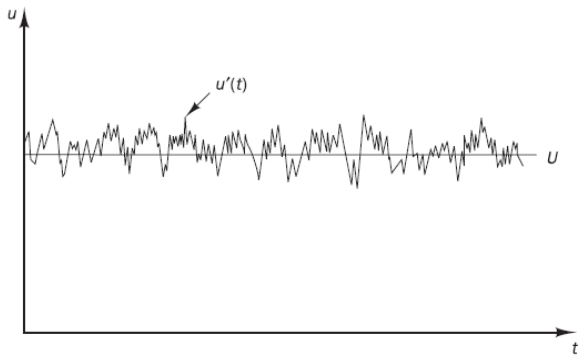

Figure 12 Turbulent flow regimes (Oslen, 2011)

Turbulent kinetic energy (TKE)

Turbulent fluctuations always have a three dimensional spatial character given as u', v',w'. The fluctuations are calculated as a standard deviation of the measured velocity in the various flow directions. Turbulent kinetic energy per unit mass at a particular point is then defined by the following equation: (Versteeg and Malalasekera, 2007).

$$k = \frac{1}{2}(\overline{u'^2} + \overline{v'^2} + \overline{w'^2}) \tag{3.2}$$

Turbulence Intensity

Similarly, the turbulence intensity, T_i, is defined using the average root mean square velocity and is defined as follows:

$$T_i = \frac{(\frac{2}{3}k)^{1/2}}{U_{ref}} \quad (3.3)$$

Here, U_{ref} is the reference mean velocity at a particular point.

Vorticity

Swirling motion in turbulent flows can also be characterized using the concept of vorticity, which is defined by the curl of the fluid velocity along the fluids axis of rotation.

3.1.3 Settling Basin Design

Settling basin as depicted in Figure 13 is usually the most efficient way to handle suspended sediments in headworks arrangements. Data from sediment studies are used for the optimal design of settling basin. A general design criterion for most HPP in Nepal is the exclusion of all sediments with a diameter greater than 0.15 mm to 0.30 mm.

Figure 13 Sediment deposition in the settling basins of Khudi HPP

Settling basins uses the principle of enlarged channels after the water has been diverted from the river. The reduction in water velocity causes the settling of the sediments in the basins by gravity. HPP maybe partially closed depending on the level of sediment concentration in the turbine flow and performance of the basin affecting the regularity and the power production of the plants.

As the main objective of the settling basin is to reduce the turbulence level in the water to allow sediment to settle in the basin, it is crucial that the flow velocity in the settling basin, which is called transit velocity, is low. Turbulence near the intake will reduce the performance level of the settling basin, which in return will affect the regularity of the plant and its efficiency. The hydraulic performance of the settling basin needs to be conducive for sediment in order to attain the required sediment exclusion.

There are several methods for computing the trapping efficiency of a settling basin. A particle approach to trap efficiency as in the Camps or Shields method, which are analytical methods, computes the probability of a single particle being trapped in the settling basin as described in Lysne et al. (2003). Camps diagram includes the effect of turbulence on the fall velocity of the particles, where the fall velocity and thereby the trap efficiency increases with decrease in turbulence level in the flow. Similarly, Vetter uses sediment concentration and flow distribution as design criteria to evaluate the performance of the settling basin. Vetter's approach takes into consideration the difference in average sediment concentration in the inlet flow to the settling basin and the outlet flow from the basin.

Settling basins are recommended to have at least two chambers separated by longitudinal divide walls, such that inspection and maintenance can be carried out in one of the basins during the dry seasons without affecting the operation of the power plant.

The hydraulic design of a settling basin arrangement needs to secure the following (Lysne et al., 2003) :

- An even flow distribution between parallel settling basins for various flows
- An even flow distribution internally inside each basin for various flows
- Efficient removal of deposits during flushing of the basin

Size and shape of the basin are the major factors affecting its trap efficiency. A larger basin helps in increasing the amount of sediments excluded and a good shape of the basin produces even flow distribution in the basin increasing its trap efficiency. The major components of a typical settling basin are shown in Figure 14.

In order to achieve an even and optimum flow distribution along the basins guide walls are commonly used at the inlet transition and slotted walls at the outlet. The inlet transition and expansion is recommended to have a symmetric layout with the length of the approach canal mounting to ten times the width of the canal upstream of the expansion towards the settling basins. This helps to avoid the effect of secondary currents, rotational flows, set by a bend in the

approach canal and to ensure that the velocities at the inlet are maintained in the range, 1.1 to 1.3 m/s.

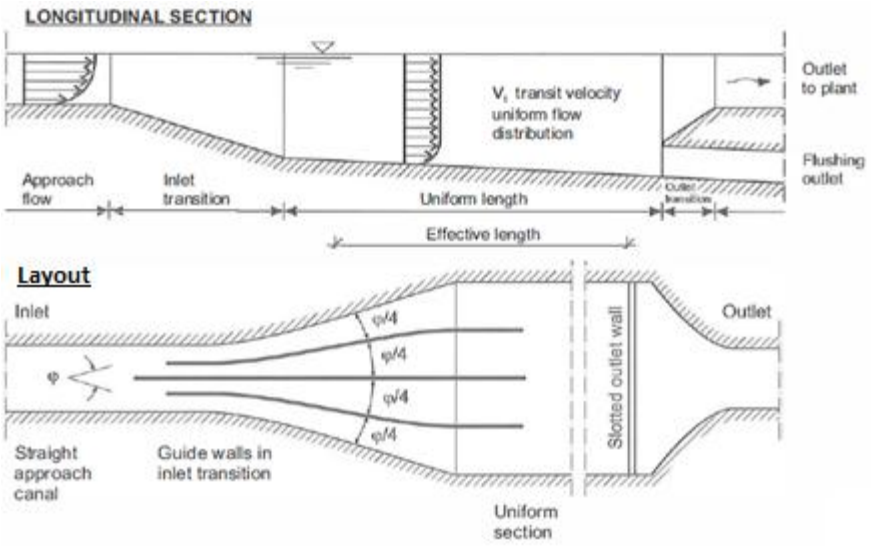

Figure 14 General layout of settling basin (Lysne et al., 2003)

A smooth and symmetric expansion including a small opening angle (ϕ/4), less than 10 to 12 degrees, with the help of guide walls prevents the separation of flow at the inlet transition. If the topography does not favor a symmetric design, then pressurized canals can be used to accelerate the flow downstream of a bend such that effects of secondary currents are nullified.

Flow tranquilizers, as shown in Figure 15, are filters where the flow is distributed over a cross-section by the use of head-loss. They are also used to replace long and gentle inlet transitions. However, both slotted outlets and tranquilizers lead to an extensive head-loss and will lead to generation loss throughout the lifetime of the plant and need careful consideration and optimization before usage (Lysne et al., 2003).

Figure 15 Flow tranquilizers at the inlet of Settling basins in Lower Modi HEP

3.2 Model theory

Physical hydraulic model (PHM) studies in general use reduced topographic and structural scale. In order to gain comparable results between the prototype and the model, scaling ratios of motion, forces and geometry needs to be maintained. This is known as the law of similitude.

The geometric similitude, the similarity in form, is satisfied when the ratio of all corresponding length, L, dimensions in the model and the prototype are the same and can be given as follows:

$$Lr = Lm/Lp \tag{3.4}$$

Here, index r denotes ratio whereas m and p respectively denote the model and prototype.

The kinematic similitude is obtained when all the forces at geometrically equivalent points have similarities in motion, constant velocity, v, and acceleration, a.

$$Vr = Vm/Vp \tag{3.5}$$

Dynamic similitude furthermore requires that the forces have same relative directions and can be reduced by the same scale ratio and is a perquisite for physical modeling.

$$Fr = Fm/Fp \tag{3.6}$$

The dynamic laws of similitude are derived using Newton's second law of motion through a dimensional analysis ensuring that there is a constant model-to-prototype ratio of all masses and forces acting on the system.

$$F = m * a \tag{3.7}$$

The most common law used in hydraulic modeling is named Froude's model law, which is used in the development of all physical hydraulic model studies conducted in this work, and is deemed relevant for discussion.

$$\sqrt{\frac{\vec{F}_i}{\vec{F}_g}} = \sqrt{\frac{inertial\ force}{gravity\ force}} = \sqrt{\frac{\rho L^2 V^2}{\rho L^3 g}} = \frac{V}{\sqrt{gL}} = Fr \tag{3.8}$$

The Froude law relates gravity and inertial forces, using the Froude number (Fr) and neglects viscous forces and surface tension forces. River with free water surface flow are gravity driven, turbulent (Reynolds number, Re>2000-3000) and incompressible in nature due to which the almost all the models of rivers and hydraulic structures are based on the Froude model law.

Following scale ratios, as shown in Table 3, are generated using the Froude model law:

Table 3 Scale ratios for various parameters when using the Froude model law (Lysne, 1982)

Parameter	Unit	Relative scale
Length	m	L_r
Velocity	m/s	$L_r^{1/2}$
Time	S	$L_r^{1/2}$
Discharge	m^3/s	$L_r^{5/2}$
Area	m^2	L_r^2
Volume	m^3	L_r^3

However, some practical aspects and limitations of using a single model law needs to be considered. When using only one model law, the model is incapable of simulating all relevant forces in the model at the proper scale. For example, it would be difficult to maintain the turbulence in the river during dry season in some rivers such that the viscous forces and the surface tension forces cannot be neglected. Similarly, air entrainment effects in the prototype cannot be modeled using the Froude law. Laboratory effects due to the limited space, model constructability, lack of instruments in the laboratory also needs to be considered and the model structure needs to be optimized accordingly.

Moreover, Froude's model law is valid for sediment particles with a grain size up to 2.00 mm -3.00 mm based on Shield's experiments. The law is still applicable but with inaccuracies for smaller grain sizes up to 0.20 mm. For particles smaller than 0.20 mm modeling becomes very complex as cohesive forces between the particles dominate the grain stability. The sediment particles are modeled with the selected scaling ratio based on sediment measurements and estimates made for the prototype. As the rate of sediment transport does not follow the Froude's model law the amount of transported

sediment in the model is not comparable to the actual prototype value but is used for qualitative information.

3.3 Numerical Modeling – CFD

With the evolution of increasingly powerful computers, numerical programs have recently emerged aiming to act as an alternative to physical modeling. Computational fluid dynamics has been attempted to predict complex water flow patterns and model sediment transport instead of physical models. The major advantages here are savings in cost and time. However, due to its limitations such as instability in calculations and difficulties in obtaining convergence, physical modeling is still preferred. A number of cases have previously been studied to develop and enhance the use of CFDs. The studies have focused on validating the numerical simulations with data from the physical models to assure its usability and sufficient quality in the results.

3.3.1 Grids

In numerical modeling, the geometry is divided into a large number of geometrical elements called grid cells, shown in Figure 16, and the equations are solved in each of these cells. The cells in the entire geometry of the model altogether form the grid and can be classified according to their shape, orthogonality, structure, formations and movements.

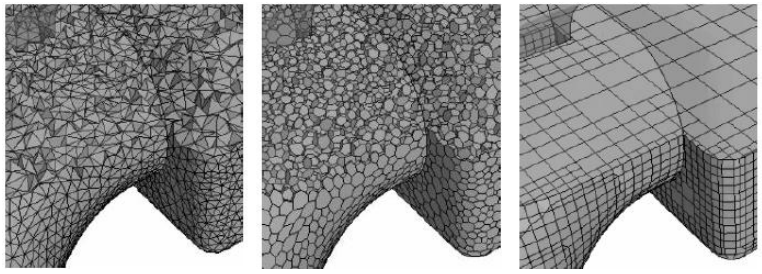

Figure 16 Different type of grid structures (Hasaas, 2012)

3.3.2 Navier Stokes equations

The Navier stokes equation is a non-linear second order differential equation based on the continuity equation and the momentum equation. The equation is used to compute water velocity in numerical models and is derived based on equilibrium forces on an infinitesimal volume of water in a laminar flow under the assumption of mass conservation.

The equation is three dimensional and time-dependent and given in a tensor notation such that the spatial variation in all directions is accounted for in the computations. The equation consists of four terms in total. The left side of the equation consists of two terms. The first term is the transient term and can be neglected during steady flow conditions. The second term describes the convection process. The first term on the right side is the pressure term and the second term is the diffusive term and includes viscosity. The application of the equation is restricted to incompressible flow and Newtonian fluids (Kettner, 2010).

$$\frac{\partial U_i}{\partial t} + U_j \frac{\partial U_i}{\partial x_j} = \frac{1}{\rho}\frac{\partial}{\partial x_j}\left(-P\delta_{ij} + \rho\nu\left(\frac{\partial U_i}{\partial x_j} + \frac{\partial U_j}{\partial x_i}\right)\right) \tag{3.9}$$

3.3.3 Discretization methods

Discretization is the transformation of partial differential equations from one cell to another, where the variable in one cell is a function of the variable in the neighbor cells. The discretization of the physical equations along the grid can be done in space and time.

Spatial discretization based on the Navier-Stokes/Euler equations can be executed in several ways. The finite difference method employs the Taylor series expansion for the discretization of the differential form of the flow variables. Finite element method uses the integral formulation of Navier-Stokes/Euler equations but can only be applied in unstructured grids. The finite Volume method, also used in Star CCM+, utilizes the conservation law- the integral formulation of Navier-Stokes/Euler equations through a finite control volume (Balzek, 2005).

The finite volume method is further categorized into several schemes based on the methods of estimating variables on the cell surfaces. A first order discretization scheme uses only one cell upstream of the cell for discretization whereas second order scheme uses two cells upstream of the cell for discretization of equations.

Temporal discretization is applied for unsteady flows, which is categorized into implicit and explicit methods depending on whether the spatial discretization is based on values in time step j or j-1. An implicit solution uses values in the former time step j, whereas an explicit solution uses time step j-1. Though the

use of explicit method is simpler, implicit method provides a more stable solution.

3.3.4 Turbulence models

Modeling turbulence in flows is a significant problem in numerical modeling and several methods are developed to model the effect of fluctuations in an approximate manner. All the available models solve the Navier stokes equations, however in different ways. As there is no exact way of modeling the turbulence, the turbulence model needs to be selected to represent the flows in reality.

- Direct numerical simulation (DNS) model uses very fine grids such that eddies are dissipated due to the kinematic viscosity in the grid. Consequently, the computational requirements are extensive. The model is also only applicable for simple flow problems with low Reynold numbers in the order 10^4-10^6 (Balzek, 2005).
- Large Eddy Simulation (LES) models uses very fine grids to solve larger eddies based in computations, and a turbulence model for the smaller structures. The spatial resolution of the grids can thus be lower than DNS and the modeling complexity and simulation costs are relatively reduced (Kettner, 2010).
- Reynolds-Averaged Navier-Stokes (RANS) equations

$$\frac{\partial U_i}{\partial t} + U_j \frac{\partial U_i}{\partial x_j} = \frac{1}{\rho}\frac{\partial}{\partial x_j}(-P\delta_{ij} - \rho\overline{u_i u_j}) \tag{3.10}$$

RANS equations are time-averaged Navier-Stokes equations for steady state situations with an additional term used to represent the transfer of momentum due to fluctuations in the water flow. The challenge lies in modeling the additional term known as the Reynolds-stress term.
Two different approaches are used in Star CCM+ to model the Reynold stress term:

1. Eddy viscosity model uses the concept of turbulent viscosity to model the Reynold stress term as the function of averaged flow variables. Boussinesq approximation is often used for modeling.

The variable k is the turbulent kinetic energy, δ_{ij} is the Kronecker delta, which is 1 if i=j and otherwise it is 0 and v_T is the eddy viscosity.

$$-\rho\overline{u_i u_j} = \rho\nu_T\left(\frac{\partial U_i}{\partial x_j}+\frac{\partial U_j}{\partial x_i}\right)-\frac{2}{3}\rho k\delta_{ij} \tag{3.11}$$

In Star CCM+ three different models that use the eddy viscosity to solve the Reynold stress term are available (Adapco, 2012).

K-epsilon (k-ε) model uses two partial differential equations, the turbulent kinetic energy (TKE) and the dissipation (ε) of TKE to solve for eddy viscosity. The eddy viscosity is modeled as an average for all three directions. Thus, although the model is not very accurate it gives a good compromise between robustness and accuracy.

K-omega model is an alternative to K- ε model and uses k and the specific dissipation rate (ω), the rate per unit TKE instead of ε to solve for the eddy viscosity. This model compared to the k- ε model has an improved performance for boundary layers under difficult conditions due to pressure gradients and is applied throughout the boundary layer.

Spallart-Allmaras model contrary to the above mention turbulence models solves only one equation, the convection-diffusion equation, for the eddy viscosity. The model is not suited for flows where complex recirculation occurs in the flow field.

2. Reynold Stress Transport model solves the Reynolds stress term by solving for all the components involved in the stress term. As a result, the model accounts for effects of anisotropy due to strong swirling motion, streamline curvature, rapid changes in strain rate and secondary flows. However, the model requires significant computational effort and time.

3.3.5 Stability and convergence

Numerical modeling is an iterative process and the initial variables need to be adjusted in order to gain satisfactory results. Convergence criteria are based on

residual values. Residual values measure either the deviation between correct values and the values in the current iteration or the difference between two simultaneous iterations. Star CCM+ uses the latter. A low residual, usually less than 0.001 indicates convergence (Oslen, 2011).

$$r = \frac{\sum_{1}^{n} |U_i - U_{i-1}|}{nU_c} \tag{3.12}$$

Instabilities occur when the residual values oscillate often and become very high. Relaxation coefficients are used to weight cell variables that are used for each iteration. The use of relaxation coefficients will give a slower convergence speed; however, it will also help to avoid instabilities. Relaxation factors are often lowered when the solution diverges because of instabilities (Oslen, 2011).

$$v = r * v_i + (1-r) * v_{i-1} \tag{3.13}$$

3.3.6 Courant Number

The Courant-Friedrichs-Lewy number is defined as follows (Courant et al., 1956):

$$C = \frac{u_x \Delta t}{\Delta x} + \frac{u_y \Delta t}{\Delta y} + \frac{u_z \Delta t}{\Delta z} \tag{3.14}$$

Here, u denotes the velocity in x, y and z direction. Δx, Δy and Δz are the cell sizes in respectively x,y and z directions and Δt is the time step between two successive computations. The courant number defines how fast a particular phase passes through a cell. If the courant number is larger than one then the velocity of particle is understood to be so high that it passes through a cell in less than the allocated time step. Thus, for a proper convergence of the solution the convective courant number for a cell should be less than one.

4 Methodology

River hydraulics is one of the major factors leading to extensive sediment transport into the waterways of a Hydropower plant (HPP) as discussed earlier. The hydraulics of the river channel at the intake is special considered in this thesis when studying the case of LMM headworks and the model studies of Khudi HPP and Kabeli 'A' HPP conducted at Hydro Lab.

Turbulent flow field near the intake and the settling basin along with the effects further downstream in the various structures is assessed with respect to performance standard of the intake as a whole. The challenges in investigating these complex flow fields and methods to diminish their effect are furthermore established. Physical model study is used to understand the flow pattern at the headworks.

The physical hydraulic model study implements the theoretical aspect of headworks design during the assessment of the performance of LMM headworks and comprises of the following parts. Based on the literature review presented as the theoretical background to this study the concept of headworks design is analyzed for the various case studies on headworks design further in this work.

The case studies includes an evaluation of the given design and improvements made on the headworks with focus on sediment handling arrangement and hydraulics, both during normal conditions and during floods. Furthermore, performance standards of the intake related to the study of flow patterns in the intake area and the settling basins; bed control in front of the intake and passage of floating debris has also been reviewed.

For the case study of LMM HPP velocity measurements has been conducted using ADV and micro propeller current in the physical model to analyze the flow patterns and hydraulics in the settling basins. The measured velocities are then used to establish turbulence levels in the water by calculating the turbulent kinetic energy. Results from the collected measurements are later used to compare against the results from the numerical simulations in order to identify the uncertainties and accuracies of a numerical model study. Uncertainties and errors from the measurements are also evaluated and discussed.

Computational fluid dynamics (CFD) model is also used as an alternative method to replicate the flow phenomenon using STAR CCM+. The reliability and the accuracy of the software used is studied and the uncertainties and limitations are identified.

The numerical model uses a 3D-Autocad model of the LMM HPP developed from the drawings provided by Hydro Lab. Headworks geometry is then imported from AutoCad into Star CCM+. Grids are generated for the model and a reference model is developed with a standard setup of mesh and physics conditions. Limitations of the numerical model including the boundary conditions are determined and required data are simulated based on the setup provided. Results are extracted and processed for comparison with the measurements conducted in the physical hydraulic model. The work is concluded with the analysis of performance of the proposed headworks arrangement with focus on settling basin for the headworks of LMM HPP along with the identification and evaluation of uncertainties and recommendations for further work.

5 Physical hydraulic model study of the headworks of LMM HPP

An efficient and proper planning and design of the various hydraulic parts of a HPP requires a hydraulic model study as it is often difficult to compute all the parameters involved and predict all the consequences. Hydraulic model of the headworks of LMM HPP is therefore used to verify the analytical design by carrying it out manually.

The Physical hydraulic model has been used to replicate flows and pressures of a water flow in a small-scale version of the topography and structure that has been studied. The structure that is to be studied is often referred to as the prototype. Model construction of the river reach and the headworks prototype have allowed the study of various parameters such as the flow pattern, slope and velocities in a visual way. Immediate visualization of the designed solutions have helped to increase the understanding of the physical processes. Extreme conditions have been simulated on the model to ensure the safe design of headworks structures. Although some simplifications are used to achieve the similitude between the prototype and the model by the use of Froude model law discussed in Chapter 3.2, a high degree of accuracy and reliability has be attained by the use of empirical rules for the interpretation of the model tests.

5.1 Model study methodology

The following general methodology have been applied when conducting the physical model study (Shrestha and Bogati, 2012):

1. Field data on hydrology, river bed material and topography are acquired.
2. The main elements of the river topography, water flow and coarse fractions of river bed material are reproduced in the scaled model. Figure 17 shows the reproduction of the river bed along with its physics for the LMM HPP: The figure to the left shows the actual river conditions whereas the right one is the model setup at Hydro Lab.
3. Calibration of the model is then done by the use of observed events during field studies. The model needs to be able to reproduce historical events such that alternative arrangements can be performed on the model.

4. Headwork structures are built in model scale and placed in the model. Performance is simulated and bed movements and flow patterns are observed and recorded under various flow conditions.
5. Problems are identified and alternative arrangements are suggested and developed with the model study consultant/client.
6. The developed concept is verified through tests and the design is optimized.
7. Tentative operational procedures can also be developed if operational aspects of the final designs are simulated.
8. Critical phases of the construction process can also be studied by rebuilding the model if needed.

Figure 17 Comparison of the model and prototype of the headworks site of LMM HPP (Shrestha and Bogati, 2012)

5.2 The initial design

In order to evaluate the general hydraulic performance of the initial design as provided by the Client a physical hydraulic model was developed at Hydro Lab in a scale ratio of 1:40. The study of the initial design is based on the report prepared by Shrestha and Bogati (2012) whereas the study of the modified arrangement has been a combined effort of the author and the Hydro Lab team working on the physical model of LMM HPP. As the model is yet to be finalized for the final design, study conducted on the model during the author's stay at Hydro Lab has been focused and analyzed. The final arrangement mentioned here is also the one that was finalized before the author's departure from Nepal.

Error! Reference source not found. gives an overview of the initial headworks area and the structures involved. The arrow is used throughout this work to denote the flow direction at the site. The initial headworks design as provided by the Client consists of an ogee shaped free overflow 45.0 m long concrete weir with the crest elevation of 2094.0 masl followed by a 52.0 m long stilling basin at an elevation of 2087.0 masl. Two bed load sluices have been placed along the forebay of the intake and the flow is diverted to a side intake consisting of four intake orifices. The orifices are further connected to two gravel traps and the water then flows through a common pressurized channel and into four settling basins, which manages the suspended sediment in the water and prevents its passage further into the waterways. A 4.80 km long tunnel then conveys water to the power house for energy generation (Shrestha and Bogati, 2012).

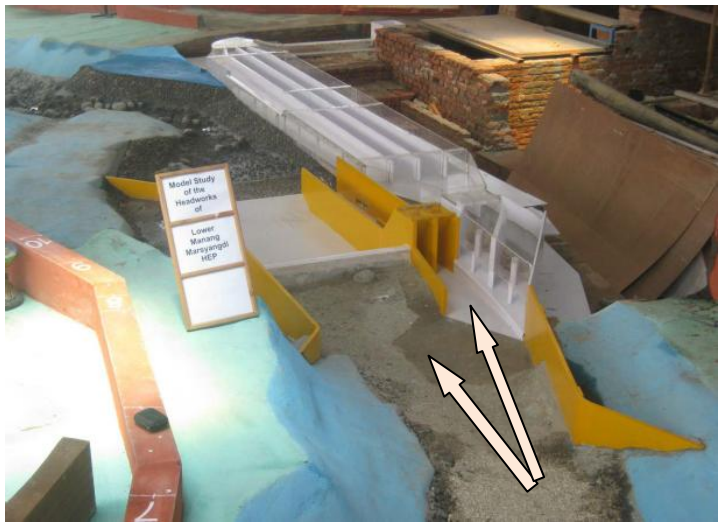

Figure 18 Initial physical model of the headworks of LMM HPP (Shrestha and Bogati, 2012)

The study assesses the performance standards of the headworks with respect to the performance standards discussed in Chapter 3.1.2. Problems that were identified in the initial design and the suggested modifications for the final arrangements have been presented below along with their evaluations. The salient features of the initial arrangement as mentioned earlier have been presented in Appendix B and have not been further discussed in this section as it is the functionalities the case study focuses on and not on the structural design itself.

5.3 Analysis of the initial design against the Final arrangement

Several steady flow situations representing various return periods of flood presented in Table 1 were tested to analyze the initial headworks design based on its overall performance. In order to represent the bed load transport in the river the model was continuously fed with sediments and gravels. Based on the observations made during the tests significant problems were noted related to the hydraulic performance and sedimentation in the vicinity of the headworks site.

5.3.1 Intake Hydraulics

The initial design of the intake was capable of withdrawing the design discharge ($52.0 m^3/s$). However, due to significant increase in velocities at higher flows shooting flows were observed at the intake gates creating upwelling and rotational flows in the gravel trap.

Slotted inlets, with a total of four intake orifices for each intake, have been provided in the final arrangement to overcome local flow circulations at the intake which leads to the gravel trap and further to the intake gates. In order to avoid upwelling and any secondary current effects at the intake the gates were adjusted downstream of the gravel traps. The gravel free discharge is now conveyed through the intake gate along the pressurized canals to the settling basins.

Figure 19 Final arrangement of the intake of the PHM of LMM HEP

The main stream flow was diverted towards the intake at almost all flows that were tested such that the intake was vulnerable to sediments and boulders. Hence, a river training structure along with a guide wall has been placed along the bed load sluice to create an outer bend effect at the intake orifices and separate the bed load sluice from the weir. Similarly, sidewalls have been placed along the right riverbank near the weir crest area to prevent erosion of the side bank and gain a uniform flow towards the intake.

Based on dye tests shown in Figure 19 some upwelling is still evident along the approach canal, however the flow is observed to be calm and uniform along the gravel trap. The turbulent flow along the stretch canal could be controlled by regulating the opening of the bed load sluice gate.

Passage of floods

The initial design of the weir as shown in Figure 18 is assessed to be capable of safely passing all flows including the design flood.

Although the energy dissipation in the stilling basin is found satisfactory, erosive supercritical flow was observed downstream of the end sill when the bed load sluices were in operation. The erosive flow had scouring effects on the boulder riprap laid downstream. This scenario was mostly prevalent for the 2-year return flood (discharge) and improved for higher flows. Due to a high flow capacity of the bed load sluice shooting flows were observed from the bed load sluiceways at higher flows (Figure 20). Thus, scouring effects were mostly concentrated on the rightmost part of the stilling basin near the settling basin wall threatening the basin's stability.

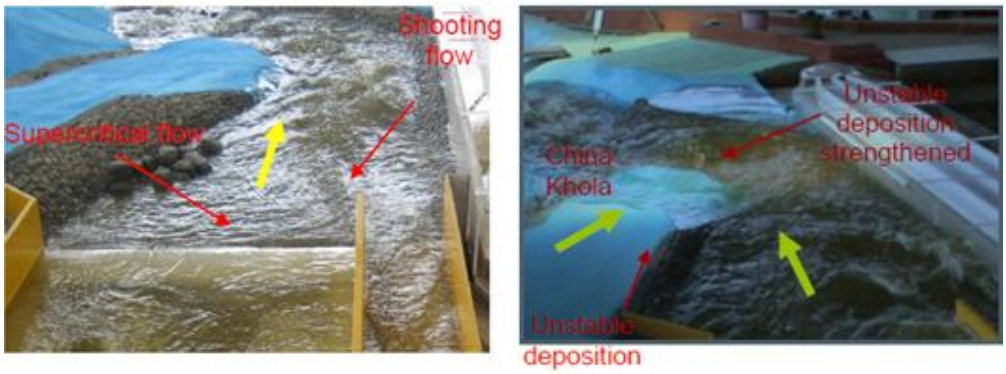

Figure 20 Problems downstream on the inital arrangenement of the PHM of LMM HPP (Shrestha and Bogati, 2012)

The fan deposit of the China Khola at the downstream end of the headworks is responsible for maintaining the tail water level. However, the deposits especially on the right bank are observed to be susceptible to erosion at higher floods and needs to be taken into consideration for further modifications.

A single bed load sluice with a relatively less discharge capacity has been adopted in the final design. Figure 21 shows an initial design of the bed load opening formed as a hopper. The design has been optimized further to the final arrangement shown in Figure 21. A flip bucket has been placed at the outlet such that the water from the gravel flushing does not mix up with the water from the bed load sluice creating turbulent flows near the stilling basin area. The fan deposit from the China Khola has been cut down and boulder riprap has been placed along the downstream river bank. The stilling basin has been deepened to provide a larger dissipation of energy and boulder ripraps have been carefully placed as protection works along the downstream river stretch until the river meets the natural terrain of China Khola. Smooth transition in river flow from the spillway along the downstream river stretch can be seen in Figure 21 during the average monsoon flood scenario.

Figure 21 Initial design of the bed load hopper

Passage of trash and floating debris

The passage of floating debris and trash above the weir and the bed load sluice was found satisfactory at all flow conditions tested in the model. Although a slight rotation and stagnation of flow was observed along the right bank where step pools were formed in the upstream section of the weir axis, trashes such as leaves and grasses were carried along with the main river flow and seldom got trapped. Passage scenario was similar for the average monsoon flow whereas for higher flows floating debris seemed to easily pass downstream with the mainstream flow.

A pressurized bed load sluice of 3.00 m×3.00 m with a hopper at the inlet has been designed for the separation of bed load sediments before the intake. The intake approach canal above the hopper allows for the passage of trash and floating debris. A flap gate is placed at the end of the intake channel with a width of 5.00 m controlling the passage of trash and floating debris coming along with the flow to the intake. Deposition on top of the slab may be

removed by a slotted pipe system or with other methods and has not been considered in the model study.

Passage of sediments

The design flow had the capacity of transporting cobbles up to 0.09 m in size. Average monsoon flow had the capacity of transporting cobbles up to 0.16 m in size. 2-years flood was observed to transport boulder between 0.60 m and 0.80 m whereas boulders up to 2.00m to 3.00 m in diameters were found transported along the river stretch during the simulation of 10-years flood.

Consequently, due to the steepness of the river and its transporting capacity mentioned above the upstream vertical face of the weir was exposed to boulders approaching at higher floods. The impact from the boulders onto the weir is expected to create severe damages.

Weir crest increment by 2.00 m to a level of 2096.0 masl helped to significantly handle the bed load sediments along the river stretch. The increment of weir crest decreases the gradient of the river and thereby the approach velocity of the river and the transported boulders. Large boulders were now observed to be transported mainly along the left bank and the fines were diverted towards the intake with the increase in river flow (Figure 23).

Bed Control at the intake

During the design flow scenario the outer bend effect was significantly noticeable near the intake area with deposition of fine sediment in the inner bend such that the right bank where the intake was proposed seemed relatively sediment free.

For flows with an additional 20% flushing discharge to the design discharge and the average monsoon flow sediment deposition was observed in front of the intake, which over time clogged the intake. Figure 22 shows building of the bed in front of the intake and its partial clogging. Thus, it was deduced that the bed load sluices had

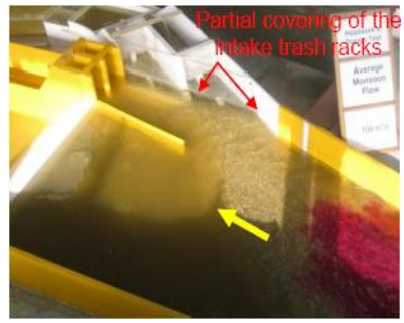

Figure 22 Bed control at the initial arrangement of LMM HPP (Shrestha and Bogati, 2012)

insufficient suction capacities at higher flows and was incapable of maintaining bed control in front of the intake.

Therefore, significant changes in the design of bed load sluice were carried out in the model. A hopper with under sluice culvert was introduced in order to increase the suction capacity and keep the intake free from bed load deposition. The bed load sluice was observed capable of handling the sediment approaching the intake (Figure 23). The hopper was optimized with respect to suction capacity and to maintain a uniform flow towards the intake. In order to increase the suction capacity of the bed load sluice both the mouth of the hopper and the river training structure at upstream has been optimized with respect to their size to constrict the flow and increase the velocity at the inlet of the bed load sluice.

Figure 23 Bed Control at the final arrangement of LMM HPP

Exclusion of suspended sediments

The settling basins are designed to trap 90% of suspended particles with size larger than 0.20 mm. When performing dye tests rotational and skewed flow distribution was noted at the inlet transition of the settling basins. The flow was dominant along the two centre basins and the velocity in flow direction along the uniform sections of these basins was relatively higher compared to the other basins (Figure 24).

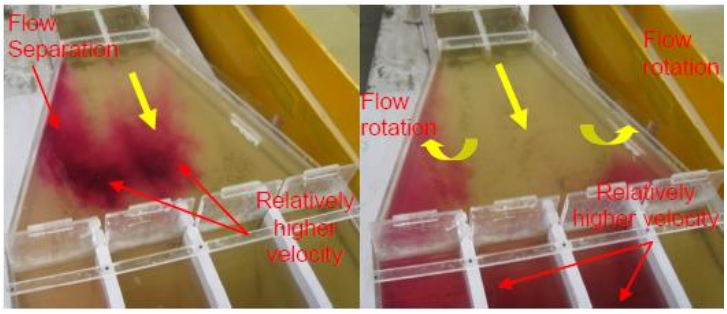

Figure 24 Settling basin inlet in the initial arrangement of LMM HPP (Shrestha and Bogati, 2012)

Similarly, uneven flow was observed at the outlet transition of the basin where the flow in the leftmost basin was almost negligible compared to the other basins (Figure 25).

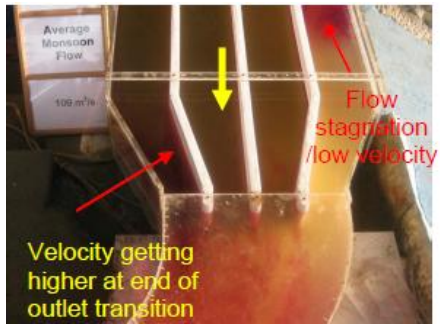

Figure 25 Settling basin outlet in the initial arrangement of LMM HPP

Based on the observed performance of the given design, the approach culvert, transition, main basins and the outlet of the settling basins was redesigned to improve the hydraulic performance. The settling basin (SB) approach channel alignment and transition sections were also modified. Alignment of single pressurized approach channel was changed by introducing two pressurized approach channels, which provided a longer transition section to the settling basins as shown in Figure26.

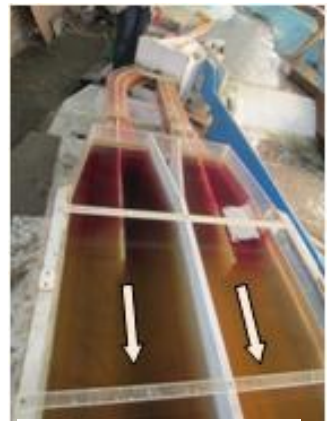

Figure 26 Final arrangement of the SB of LMM HPP

A divide wall has been provided along the approach channel until the start of the uniform section of the settling basin to avoid flow separation and maintain a uniform flow into the settling basin, designed with double hoppers. Based on the dye test shown in Figure 27 for an Average Monsoon Flood scenario relatively symmetrical and uniform flow conditions have been observed. The hydraulic performance of the settling basins was consequently improved with calm and uniform flow conditions from the start of the uniform section in the basin.

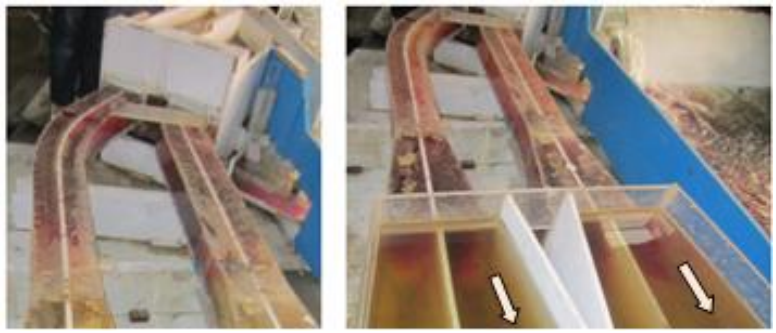

Figure 27 Final arrangement of the approach canals in the PHM of LMM HPP

The settling basin outlet design has also been completely modified. A slot of 1.00 m opening has been placed at the outlet such that the effect from the downstream flow onto the settling basin is nullified. Uniform flow conditions is now seen at the outlet transitions from Figure 28.

Figure 28 Final arrangement on theSettling Basin outlet in the PHM of LMM HPP

Flushing of settled sediments

The S4 system is planned to be used for flushing of settled sediments from the settling basin. Additional 10% of the design discharge abstracted from the river through the intake is intended to be used for flushing of settled sediments at the gravel trap and along the settling basin. Physical model study does not include the study of the S4 system and flushing of the basins and has not been assessed further in this study.

The final arrangement of the physical hydraulic model of the LMM HPP is presented in Figure 29. The design as discussed in this Chapter has shown a good conceptual performance and further optimization of the various components are currently being carried out at Hydro Lab.

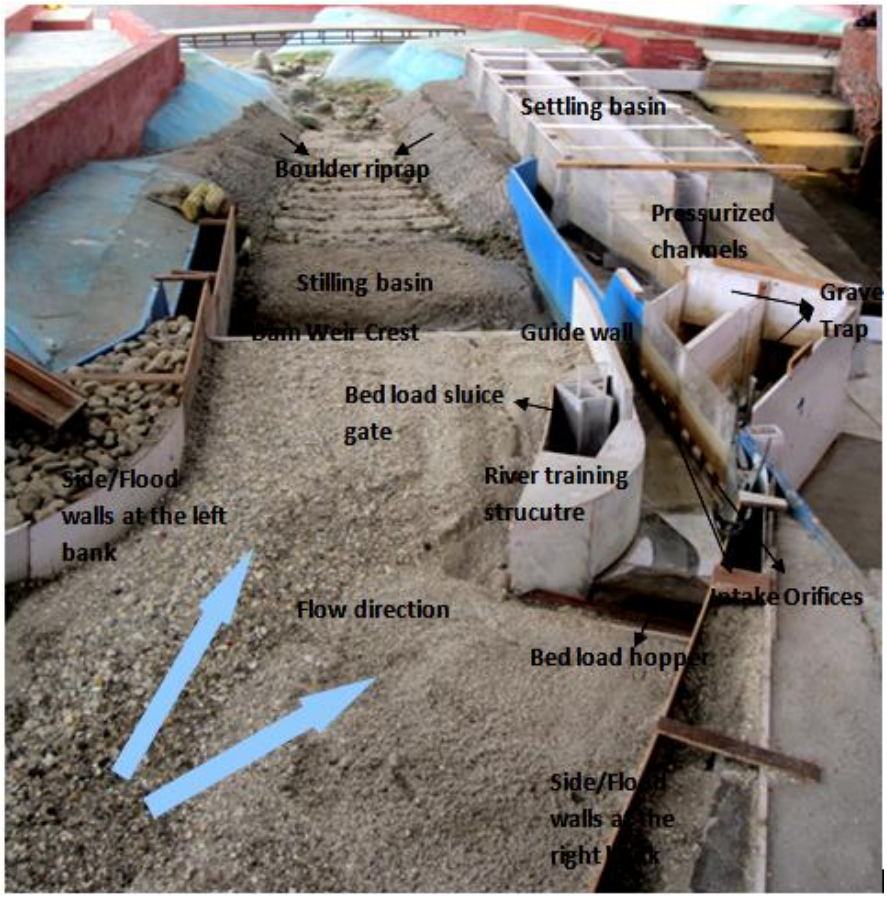

Figure 29 Final arrangement of the PHM of LMM HPP

6 Velocity measurements on the Physical Hydraulic Model of LMM HPP

In order to understand the turbulence level in the water and the hydraulics in the river that cause sediment transport it is essential to have a record of the flow phenomena in the head works structure. Numerous flow-measuring instruments with high temporal and spatial resolution have been developed like the Laser Doppler Velocimetry (LDV), Particle Image Velocimetry (PIV) and flow meter used to measure water velocities in the flow. Acoustic Doppler Velocity Meter and Micro propellers are used in this study for measuring flow velocities and are discussed below.

6.1.1 Acoustic Dopple Velocity Meter (ADV)

Flows in open channel and rivers are turbulent. It is important that velocity measurements be conducted at high frequency to resolve the small eddies and viscous dissipation process. ADV is a widely used instrument for taking velocity measurements and analyzing the turbulence level in water due to the instrument's relatively low cost, ability to take measurements at relatively high frequencies and requirement of a relatively small sampling volume. The instrument records mean water velocities in three directions with a high level of resolution and accuracy and is also capable of resolving flow turbulences(García et al., 2005). 16-Megahertz (MHz) Micro ADV as shown in Figure 30 with a side looking probe in Figure 31, produced by Sontek AS, is the velocity meter used to determine the water velocities in physical hydraulic model of the settling basin of LMM HPP.

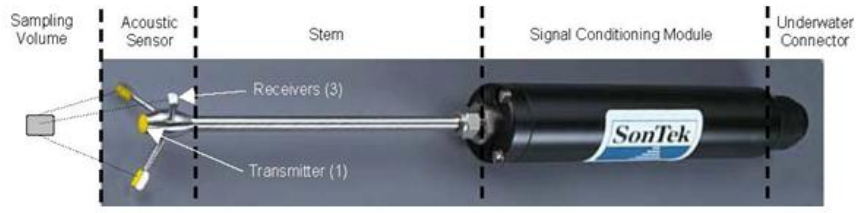

Figure 30 Standard ADV Field Probe

ADV uses the Doppler Shift principle to measure three-dimensional (3D) flow velocities. The system components include the probe, transducers, temperature sensor and an electrical module. The probe/sensor head consists

of four receiver transducers and a transmitter mounted on a cable connected to the main housing.

Figure 31 Side looking 3D probe

The device operates by emitting an acoustic signal, pulse, generated by the transmitter at a distance of 5.00-10.0 cm from the transmitter. The pulse propagates through the water column and is reflected by the particles in the water presumably moving with the flow velocity that is received by the four receiver transducers. The received signal is then used to compute a Doppler shift, change in frequency or wavelength which is introduced by the particles in motion relative to the velocimeter, based on which the velocities in the respective directions are determined.

6.2 Procedure for the ADV measurements

Velocity measurements on the physical hydraulic model of LMM HPP are taken using the Acoustic Doppler Velocimeter (ADV) and Micro propeller currently available at Hydro Lab (Figure 32). In the following sections principles of the measurement instruments is briefly explained, followed by the procedures used to conduct the measurements in the model.

Figure 32 ADV measurements along the settling basins of the PHM of LMM HPP

It is important to maintain steady flow conditions through the Settling Basin in order to have similar conditions for the different point measurements conducted using the ADV. Here, the measurements have been carried out for the Average Monsoon Flood (287m^3/s) scenario in the river with a discharge in the modeled river set to 28.36 l/s.

The gravel flushing gates need to be kept closed and the gate opening of the bed load sluice must be kept constant such that the flow at the intake does not change when measurements are being conducted. The water level needs to be

stable. Here, the water level was stabilized to the prototype equivalent level of 2097.7 masl and the bed load sluice gate was kept at a constant opening height. To prevent the impacts of wind onto the surface flow the settling basin has been covered by thin wooden planks as it got rather windy during the daytime while the measurements were taken.

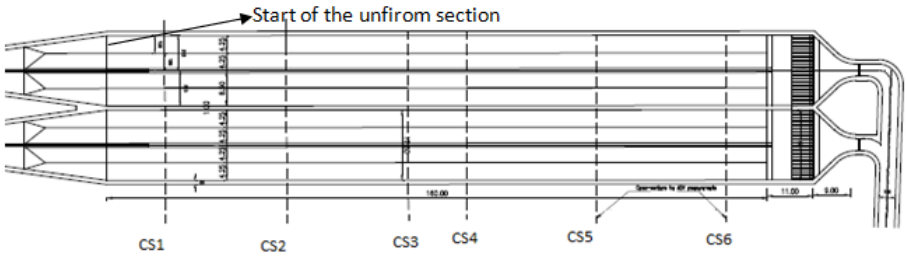

Figure 33 Measured Cross-sections along the Settling Basins of LMM HPP

Six different cross sections (CS) shown in Figure 33 and Table 4 have been decided for lab measurements along the settling basin. CS1 is the closest section and has been placed right after the start of the uniform section in the settling basin while CS6 is closest to the outlet. The sections have been divided such that the measurements give a total overview of the flow scenario in the settling basin.

Table 4 Measured Cross-sections along the Settling Basins of LMM HPP

Cross-sections	Distance from the start of the uniform section (Model values [mm])	Distance from the start of uniform section (Prototype values [m])
CS1	350	14.0
CS2	1087	43.5
CS3	1824	73.0
CS4	2174	87.0
CS5	2962	118.5
CS6	3750	150.0

The ADV needs to be configured for proper collection of data. The velocity range needs to be selected based on the expected range of data. A velocity range of 3.00 cm/s has been chosen.

For the 16MHz probe used for measurements in this work the positive z-axis is defined along the axis of the acoustic transmitter from the sampling volume towards the ADV sensor. Similarly, the positive x-axis is defined vertically down along the axis of the mounting stem from the signal-conditioning module towards the acoustic sensor. The positive y-axis is defined to give a right-hand coordinate system.
Similarly, the sampling rate needs to be selected. The sampling rate defines the rate at which the velocity data is collected. The maximum sampling rate of 50Hz has been selected with continuous sampling mode to record the fluctuations in velocity along the settling basins and develop turbulence levels in the water.

The measurements are taken for a minute at each point which gives a total of 3000 data per point. It is necessary to wait for the flow to stabilize around the ADV for some time before starting the measurements. Based on some trial measurements and the range of velocity measured it was decided to wait for about a minute before starting the measurements.

ADV measurements have also been conducted in front of the intake gate at the Gravel trap along the centre horizontal line at three different sections as shown in Figure 34 in model scale (mm). The points are numbered 1-6 from right to left bank in the direction of flow.

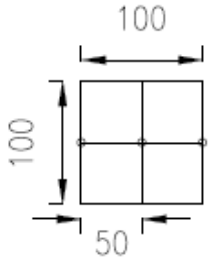

Figure 34 ADV measurements at the intake orifice of LMM HPP

The collected data files for the lab measurements are then exported using the Horizon ADV software developed by Sontek. Output files are in a tabulated format and further processing of the results is done with the use of Microsoft Excel.

6.3 Micro propeller measurements

Figure 35 Mini Air 20 Micropropeller

Velocity measurements have also been conducted using the hand held Micro propeller measurement device MiniAir20 shown in Figure 35. The measurement of flow with a propeller anemometer is considered to be a very accurate method of measurement and has an uncertainty range of 3% of the measured value. The revolution of the propeller anemometer is almost linear for flow velocity

and is furthermore independent from physical parameters such as pressure, temperature, density and humidity.

In order to understand the flow conditions at the intake orifices velocity measurements were conducted using Micro propeller. The velocity during a period of 10s was averaged to determine the average water velocity passing through the orifice. The measurements were conducted at three different points along the top of each intake orifice shown as circular points in Figure 36. The measurements here are given in millimeter (mm) based on the model scale. The intake orifices have been numbered from 1-8 in the flow direction when processing the results. In order to gain comparable results with the ADV measurements made at the gravel trap propeller measurements have also been conducted in front of the intake gate at similar cross-sections as shown in Figure 34.

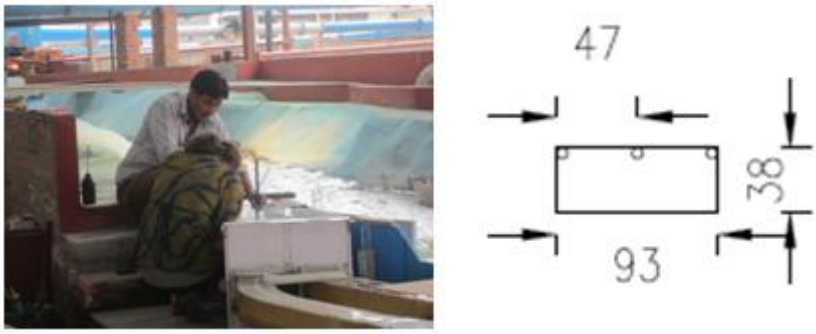

Figure 36 MicroPropeller measurements at the intake of the PHM of LMM HPP

7 Numerical model study of the headworks of LMM HPP

The Numerical model study requires the usage of two different software programs. AutoCAD has been used to replicate the 3D geometry of the physical hydraulic model (PHM) of LMM HPP based on the 2D plan drawings obtained from Hydro Lab shown in Appendix D. The numerical model has the same scale ratio as the PHM of 1:40. The geometry has been developed as an STL (stereo lithography) format such that it is supported by STAR-CCM+, in which the simulation has been performed.

7.1 Star CCM+

The numerical simulations made in this report have been performed using the Star CCM+ version 7.04.011 developed by CD Adapco. The spatial discretization is done based on the Finite volume method and can handle structured and unstructured grids. Surface repair tools in the solver allow for the processing and simulation on the geometry extracted from AutoCAD files in order to enhance the quality of geometry in the model. The program has an automatic meshing technology and mesh models. Similarly, a range of physical models with respect to time, solver, flow phases and turbulence models are provided that can be combined depending on modeling needs.

Furthermore, plots and scenes of the results can be developed post simulation in order to analyze and get a comprehensive visual understanding of the model results. These results can be tabulated and exported if necessary. The program uses a client-server architecture based on Java which handles the user interface. The server, which computes the simulations, can run in serial or parallel both with and without the client (Adapco, 2012).

7.2 The numerical model setup

7.2.1 Pre-processing

The imported stl-file from AutoCAD, as shown in Figure 37, provides the program with the necessary geometry to start the numerical model study. As the numerical model is drawn in the model scale ratio of the PHM the basic unit used for drawing is millimeter (mm) scale. The co-ordinate system in the model is defined such that the positive x-axis represents the direction of flow. The

motion from the right settling basin (SB) bank to the left SB bank defines the positive y-axis. Similarly, the positive z-axis is defined upwards in the model. The reference level is set at 2000.0 masl such that a level of 2097.0 masl in the prototype is given by the following z-axis co-ordinate in the numerical model shown through calculations below:

2097.0 masl – 2000.0 masl = 97.0 m in the prototype and is equivalent to 90 000 mm / 40.0 = 2250.0 mm = 2.25 m.

The initial purpose of the study is to develop a stable and convergent model based on standard values. This model is then used as a reference to make further evaluations and comparisons by changing the various input parameters to develop the final setup.

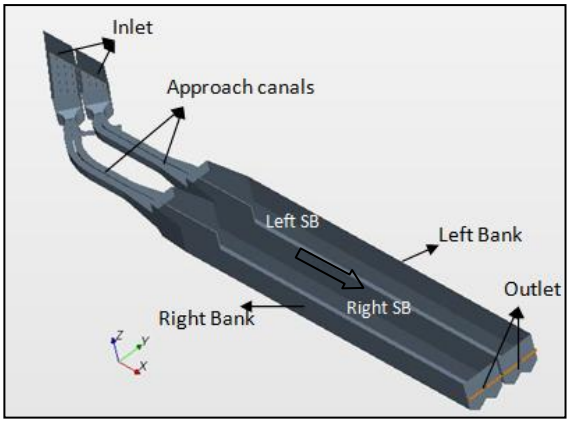

Figure 37 Imported geometry from AutoCAD; x-direction shows the direction of flow

The imported geometry requires pre-processing before the model is ready for a numerical simulation. The geometry is initially defined by a surface mesh using faces (triangles), vertices and edges. The geometric parts therefore require divisions into different part surfaces in order to set boundary conditions and do a proper meshing. The geometry is split into part surfaces, which creates parts based on angles between faces in the geometry, and the parts are merged and renamed according to their purpose (Figure 38).

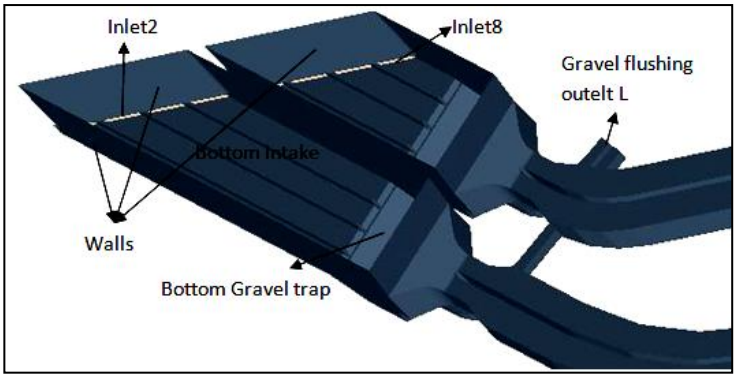

Figure 38 Surface parts in the NHM

Furthermore, the surface needs to be examined for serious errors (Figure 39). Surface diagnostics is used to repair the surface mesh to ensure that the number of pierced faces, free edges, non-manifold edges and non-manifold vertices are zero. Non-manifold edges are not shared by more than two triangles. Poor quality faces were also observed due to the triangles used in creating the shape of the surface since certain parts of the surface geometry had very sharp angles. However, they were not considered to be problematic for further simulations and have not been repaired.

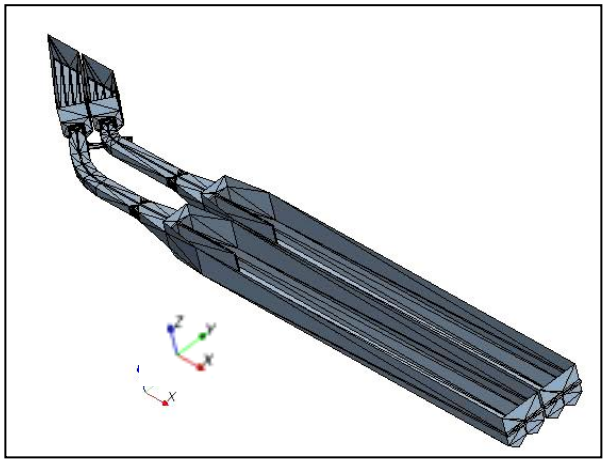

Figure 39 Surface diagnostics of the NHM

The different geometric parts are then assigned into regions such that computations could be made in the various parts. A region is assigned for each part. Similarly, a boundary per part surface is selected for the creation of boundaries for each part surface. A feature curve per part curve has been

selected to define the sharp edges and the surface details that need to be maintained in the final volume mesh.

The continuum of the model i.e. the mesh generation and the physics of the model were then selected along with the boundary conditions in order to create a functional model.

Mesh generation

A mesh continuum is a collection of the meshing models used to generate mesh for the input geometry. Two different types of mesh models are available: surface mesh and the volume mesh. The generation of the surface mesh improves the triangulation of the surface in addition to the surface repair such that a higher quality mesh is obtained. A high quality generation of a volume mesh is therefore highly dependent on the quality of surface mesh. A surface wrapper is used when the imported geometry is of extremely poor quality and creates a closed surface. The quality of the model has been increased after the surface repair and therefore a surface remesher is selected to re-triangulate poor quality closed surfaces. Table 5 gives an overview of the selected mesh models.

Table 5 Overview of the selected mesh models

Mesh type	Selected meshing models	Alternative mesh models
Surface mesh	Surface remesher	Surface wrapper
Volume mesh	Trimmer	Polyhedral mesher Tetrahedral mesher Thin mesher

Trimmer meshing model is composed predominantly of hexahedral cells with trimmed cells next to the surface and are based on orthogonal mesh structure. Trimmed cells are polyhedral cells that are usually recognized as hexahedral cells with one or more corners and/or edges cut off. Tetrahedral model comparatively is the fastest method for mesh generation and uses the least amount of memory. Thin model is suited for thin geometries as the cell shapes are decided accordingly. Polyhedral mesh type develops significantly fewer cells than a tetrahedral model and is finer close to the geometries. Trimmer model being a combination of polyhedral and hexahedral cells provides the basis for

the development of a high quality grid and has therefore been selected (Figure 40).

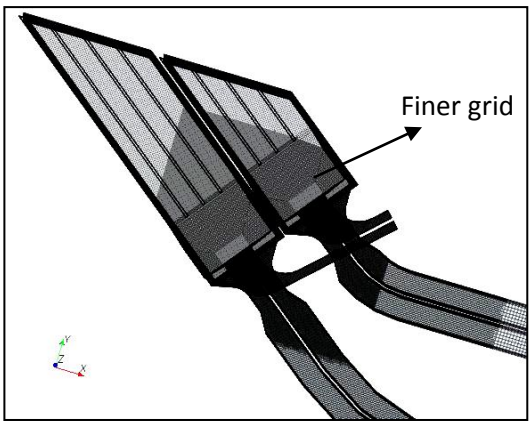

Figure 40 Volume mesh at the intake

Inputs regarding the surface cell sizes is then required for grid generation. Through a process of trial and error based on a visual evaluation of the grid quality, reference values for the cell sizes were chosen for the model. A base size of 0.10 m is selected and all the other meshing values are set relative to the base size. The maximum cell size is given as 20% of the base size and the minimum cell size as 5% and a desired surface size given by the target size as 10% of base size. Thus, a 1.00 m maximum cell size, a relative target size of 0.50 m and a minimum cell size of 0.25 m have been selected for the reference model. In addition to this, volume shapes have been developed along certain parts of the model to get a finer grid generation within these volumes. Refinement of the mesh has been done by creating volume shapes at the inlet, the gravel trap and transition to the pressurized channels, the outlet and along the settling basins at the level where there is a volume transition from water to air. The relative target size here is set to 5% of the base size. A total of 6 355 171 cells were generated in the mesh and used for further computations.

Physics of the model

The selection of various physical phenomena describing the model is done using the physics continua. Default reference values have been used to model physical phenomena such as allowable density, viscosity, specific heat , reference pressure which in this case is set to atmospheric air pressure. In addition to this a set of initial conditions need to be provided for the model to

run. For unsteady-state simulations the converged solution is dependent on the initial properties in the model and affects the path to convergence and the computational effort required. Standard constant values enabled in the model have been used as reference values for the initial conditions of pressure, turbulence and velocity. The initial water level in the model is set using a field function to gain the desired water level that is based on the lab measurements. Field functions allow for the creation of a function which is used to describe the flow conditions in the model. A field function called the initial water level was therefore established:

($$Position[2]<=2.4425)?1:0

Here, Postion [2] is the z-direction of the model with upwards direction defined to be positive. According to the function, the initial water level is set at 2.4425m and the presence of water is defined beneath and at this level in the model volume.

Table 6 gives an overview with a general description of the selected models with the alternatives available in STAR CCM+.

Table 6 Overview on the selected physics model

Type of model	Selected model	Description	Alternatives
Space	3D	Works on 3D meshes	2D, Axisymmetric
Material	Multiphase mixture	Eulerian Multiphase model (air and water)	Gas, Liquid, solid, Multi-component gas, Multi-component liquid
Multiphase model	Volume of Fluid	Simulate flows of two immiscible fluids, air and water	Multiphase Segregated Flow
Equation of State	Constant Density	The density of the fluid is invariant throughout the model	Ideal Gas, polynomial density
Time	Implicit Unsteady with a second order temporal scheme	Controls the update at each physical time to obtain convergence	Explicit unsteady, Harmonic balance, Steady
Viscous regime	Turbulent	Represents flow in continuous instability both in time and space	Laminar, Inviscid
Reynolds averaged Turbulence	K-Epsilon turbulence model with Two layer All y+wall treatment	Provides a good compromise between robustness, cost and accuracy	K-omega turbulence model, Reynold stress turbulence, Spalart-Allmaras Turbulence
Flow	Segregated flow	Used for incompressible flows with constant density	Coupled flow

Boundary conditions

The various surface parts when assigned to regions are developed as boundaries. Boundaries are lines that surround and enclose these surface parts. The various boundaries are assigned to boundary types based on the desired physics for these boundaries. The boundary-types used in this model are mass-flow inlet, pressure outlet, and walls. The mass flow inlet boundary is used for incompressible flows to represent physical conditions such as flow direction-, turbulence-, and velocity specification at the inlet when the mass flow rate is known.

Wall boundary types are impermeable surfaces. Pressure outlet boundary is used when the pressure is specified and is used in combination with mass-flow inlet. The passing water then has no influence on the flow upstream the outlet and the mass-flow at the inlet is equivalent to the mass flow sum at outlet when the model is converged. For the model in question, a mass-flow inlet has been assigned to inlet boundaries. The outlet and the top is set as a pressure outlet while the rest of the boundaries is selected to be walls and have similar physics as the bottom of the model.

Boundary conditions are then specified for each of the boundary types. **Error! Reference source not found.** on the next page gives an overview of the boundary conditions selected for the various boundary types along with alternative methods that could have been used.

The values for the wall boundary types are similar where default values have been used to define the blended wall function for walls with no slip conditions. Default values based on the physics continua have also been used to describe the physics of the outlet and the turbulence of the inlet. The turbulent intensity is set as a lower limit of 0.01 and a turbulent viscosity ratio is set to 10.0 at both the inlet and the outlet. Pressure at the outlet is set using a field function to gain a correct pressure level above the slotted outlet. Field functions allow for the creation of a function, which is used to describe the flow conditions in the model. A field function called the pressure outlet was therefore established:

$Density*9.81*(2.4425-$$Position[2])

Here, Position [2] is the z-direction of the model with upwards direction defined to be positive. According to the function, the pressure at the outlet is

equal to the pizeomteric pressure head from the position of the water level set at 2.4425 m.

There is a slight head difference at the various intake orifices due to the sloping of the approach canal. Values of the mass flow magnitude, therefore, differ for the various inlet orifices. The inlet discharge in the model and the inflow discharge in the field measurements need to be similar in order to gain comparable results from the model simulation. Thus, inlet velocity measured with micro propellers is used to calculate the mass flow rate for the eight different openings at the intake. The flow direction at the inlet also needed to be specified as the intake is placed at an angle of 142 degrees compared to the direction of positive y-axis. Flow direction values were thus calculated in the x- and y-axis to gain a correct inflow simulation.

Derived parts

Derived parts are parts created based on the input from the already existing part surfaces. Derived parts in the model are used to create streamlines along the entire geometry. Streamlines define the path of the fluid along the model based on its velocity. Derived parts are also used to create point probes for the points from which simulated data are later exported in order to be compared with the lab measurements. Six different sections, shown in Figure 41, each with six point probes along three different levels have been used from the settling basins in the numerical model. Comparisons with the lab measurements will be made along these sections. The points along each section have been created so that points along the width of the settling basin are similar to the measured and processed lab values. Plane sections have also been created at the three different levels to get a visual understanding of the inflow condition along these sections.

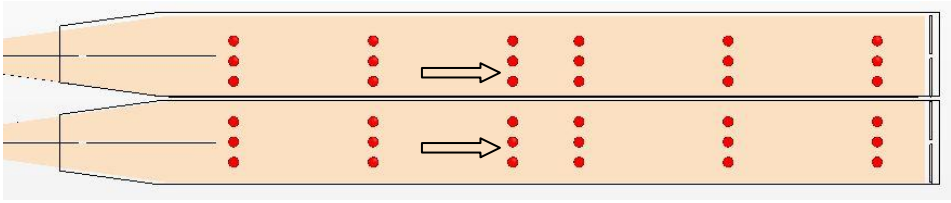

Figure 41 Derived parts in the NHM

Table 7 Selected boundary conditions

	Boundary Type	Physics conditions	Selected method	Alternatives
Intake Inlet	Mass flow inlet	Flow direction specification	Components	Boundary-Normal, Angles
		Turbulence specification	Intensity + Viscosity ratio	K+epsilon, intensity + length scale
		Velocity specification	Magnitude + Direction	Components
Settling Basin(SB) Outlet	Pressure outlet	Backflow Direction specification	Boundary-Normal	Extrapolated
		Target mass flow option	Disabled	Enabling the option
		Turbulence specification	Intensity + Viscosity ratio	K + epsilon, intensity + length scale
Top	Pressure outlet	Only mesh conditions as specified in the mesh continua	None	None
Bottom	Wall	Shear stress specification	No-slip	
		Tangential velocity specification	None	
		Wall surface specification	Smooth	Rough

Solvers and stopping criteria

Solvers are used to control the solution and are activated per iteration. The solver is automatically selected in Star CCM based on the physics models that have been selected. The difference between a solver and a model (mesh model and the physics model) is defined by their limitation to the continuum. The scope of the model is limited to the continuum selected whereas solvers can be activated over the specified continua. Table 8 gives an overview of the solvers

used and the under-relaxation factor associated with each of the solvers. The under-relaxation factors affect the convergence time and the number of inner iterations required. A reduction in the under-relaxation factors leads to an increase in the needed solution time for convergence and an increase in the number of inner iterations.

Furthermore, stopping criteria are selected to limit the simulation run-time and specify the conditions needed to stop iterating. The stopping criteria is evaluated by the simulation model for each iteration and is stopped when the criteria is satisfied. For an unsteady state model, which is used in this simulation, the stopping criteria can be given by the maximum number of inner iterations, maximum physical time or by the maximum number of steps. The maximum number of iterations has been decided by evaluating the convergent properties of the model and is set to 220000. The physical time step is set to 0.0015 s and the maximum number of inner iterations is set to 10 and involves for each physical time-step the number of inner iterations required to converge to a solution for a given cell.

Table 8 Under-relaxation factors used in the numerical model

Solver types	Under–relaxation factor
Segregated flow velocity solver	0.8
Segregated flow Pressure solver	0.2
Segregated VOF solver	0.9
K-epsilon turbulence solver	0.8
K-epsilon turbulent viscosity solver	1.0

7.2.2 Post processing

Visualizing the solution

A visual analysis of the solution data in the model can be made in the graphics window with the help of plots and scenes. Four different scenes including an empty scene alternative are available in the program feature. The geometry

scene gives a view of the surface geometry. A mesh scene provides the same visual as the geometry scene with enabled grid. Scalar scenes are used for viewing scalar fields such as the velocity magnitude total pressure and vector scenes for vector fields.

Plots based on reports of the simulation are also useful for analyzing solutions. Mass inflow monitor plots have been used to decide the inlet velocity for the model. The model velocity is adjusted such that the inflow stabilizes at $0.00689 m^3/s$. The sum of mass flow is monitored to stabilize around zero such that all incoming flow finds its way through the outlet. Similarly, residual plots have been created to evaluate the stability and convergence of the model.

Result extraction

Velocity distributions in the various directions along with the turbulent kinetic energy and vorticity have been extracted and tabulated for all the point probes shown in Figure 41. The solution data from the simulation is exported into Microsoft Excel and formatted and tabulated in a similar way as the velocity measurements conducted in the physical hydraulic model of LMM such that the two values become comparable. The points have been compared and analyzed by using both graphs and plots in Chapter 8 and Chapter 9.

8 Results

In this chapter results from the numerical simulation and velocity measurements conducted in the physical hydraulic model of the headworks of LMM are presented. Results and the uncertainties that follow are further discussed and analyzed in Chapter 10.

8.1 Results from the numerical simulation

In order to ensure that reliable results are achieved from the numerical simulation, the convergence and mass flow balance from the simulation is evaluated before presenting graphs and scenes showing the solutions from the numerical simulation.

8.1.1 Reliability and convergence of the numerical simulation

Figure 42 below illustrates the development of residuals in the numerical model with the iterations computed. The model is assumed converged when the continuity residual is less than 0.001. The residual values fluctuate over an average value of less than 0.001. From Figure 42 we see that the iterations seem to have converged after 150 000 iterations over a value of 0.0001. To ensure its consistency, however, the model has been enabled to run up to 220 000 iterations. The elapsed solution time for the unsteady simulations performed is 33s. The solver iteration elapsed time is 0.217s per iterations, which shows how long it took to execute each iteration giving a total solver elapsed time of 15 hrs for the modeled simulation.

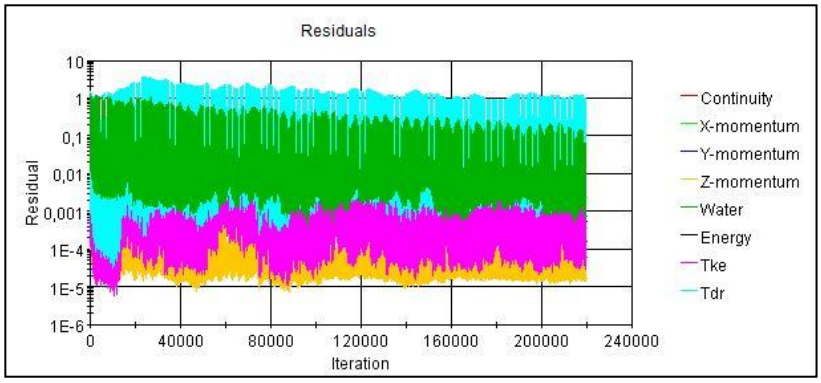

Figure 42 Residual plot of the numerical simulation

Residual monitor plot is a very useful tool in judging convergence. However, it is also important to understand the limitations of residual plots and cannot be relied as the only measure of convergence. The residual decrease is strongly influenced by the selection of physics and the initial conditions. If the initial guesses satisfy the discretized equatins the residuals may not drop at all. Errors in residuals are also dependent on the discretization scheme. The second order upwind scheme used in this simulation are associated with dispersive errors that produce residual plots that are naturally stabilizing and do not decrease montonically. The tolerance limit for the residual plot is also a subjective choice which is dependent on whether the user chooses to accept the solution according to their requirements. Similarly, the residuals also do not necessarily relate to quantities of engineering interest such as forces, pressure and mass flow rates, which helps to examine the solution and judge the convergence as the simulation proceeds.

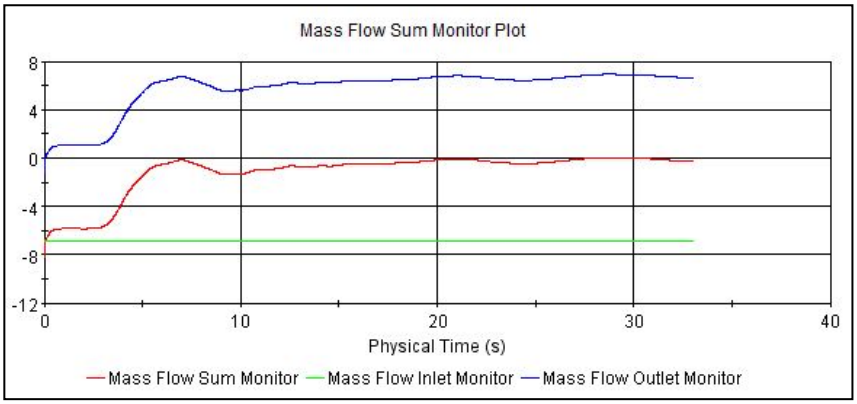

Figure 43 Mass flow plot of the numerical model

Figure 43 shows the mass flow plot of the numerical model of LMM headworks as modeled in this work. The degree of convergence can here be analyzed by looking at the mass flow sum plot. The mass flow sum here appears to stabilize around zero and a deviation of 0.500kg/s is accepted which is a deviation of about 7% from the actual desired inlet/outlet flow of 6.89kg/s model value.

8.1.2 Streamlines

Figure 44 gives an overview of the development of streamlines in the model by following a particle's motion from the inlet of the model to the outlet. We see that the velocity is highest at the inlet and along the gravel trap. The flow

entering the settling basin appears relatively uniform and the flow along the settling basin seems symmetrical. The flow at the inlet and in the gravel trap seems to be highly turbulent. Swirling and rotational motion is also observed at the inlet of the settling basin, however the motion is relatively calm further along the settling basins.

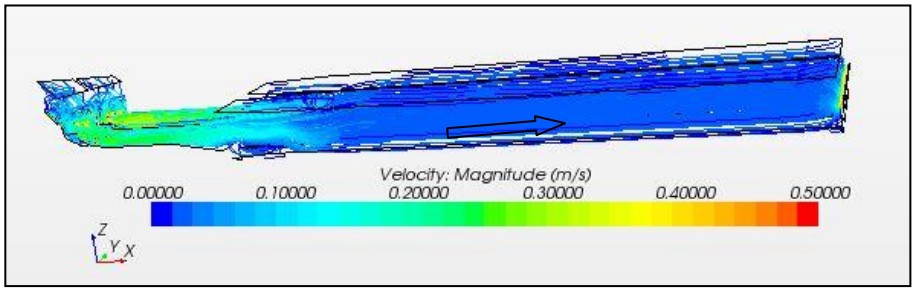

Figure 44 Streamlines of the numerical model

8.1.3 Pressure

Figure 45 illustrates the pressure development across the numerical model. It is important to check how the hydrostatic pressure builds up in the model and whether it is built in a consistent way throughout the model. Atmospheric pressure has been achieved here along the volume of the model filled with air shown by the presence of blue colour in the figure below. A smooth hydrostatic pressure development as required has been numerically simulated and has helped to analyze the results and ensure its consistency.

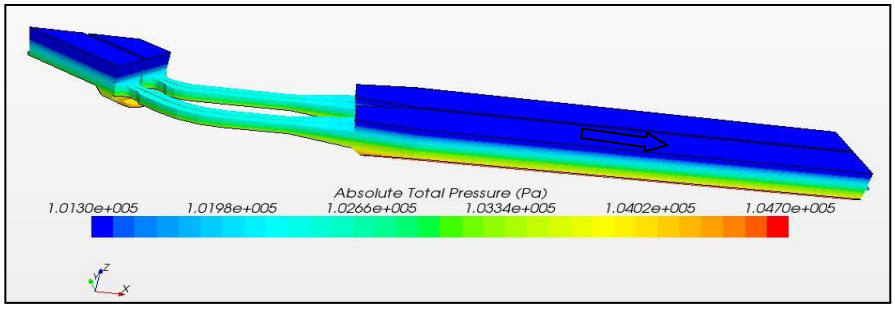

Figure 45 Pressure development in the numerical model

8.1.4 Velocity distribution

Figure 46 shows the distribution of velocity along a plane section in the model. As seen from the figure, the numerical model has not been capable of entirely simulating the velocity distribution along the gravel trap. The velocities along the gravel trap are very high in some cells and can be seen in further detail in Figure 58. The mesh quality along the gravel trap probably influences the results greatly and a finer grid may have solved the problem, which due to time constraints has not been checked further. However, the flow fields in the gravel trap are not considered to influence the velocities further in the settling basin as a stable, uniform flow in the range expected is observed along the pressurized section. The approach velocity seems relatively symmetrical and uniform. A calm flow is observed along the settling basin with negligible fluctuations in velocity. Desired flow is achieved along the settling basin, which is discussed further in this chapter and has been further analyzed from the turbulent kinetic energy values and tabulated velocity vectors in Chapter 9.

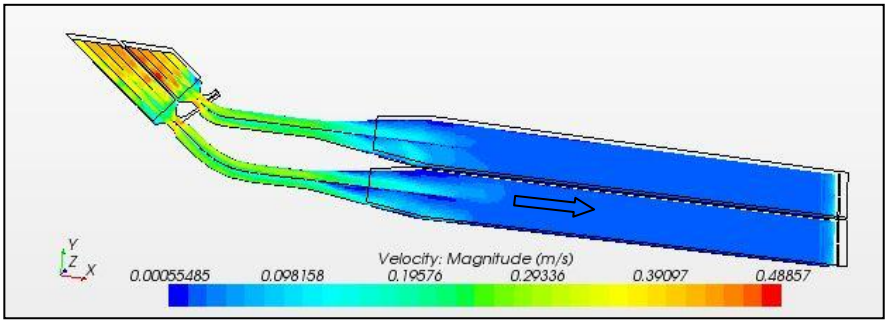

Figure 46 Velocity distributions along a plane section in the numerical model

8.1.5 Turbulent kinetic energy (TKE)

The turbulent kinetic energy as can be seen from Figure 47 is significantly higher at the inlet and along the gravel trap with a maximum TKE value of 0.003 J/kg . TKE in the left approach canal in the flow direction seems to be slightly higher though in the same range of magnitude suggesting skewed flow in the pressurized section. However, the flow is rather symmetrical and uniform along the inlet of the settling basins. Similarly, the turbulent kinetic energy is observed to have decreased significantly from Cross-section 1 to Cross-section 2. The turbulent kinetic energy also seems to have stabilized from Cross-section 2 and equivalent along the length of the settling basins.

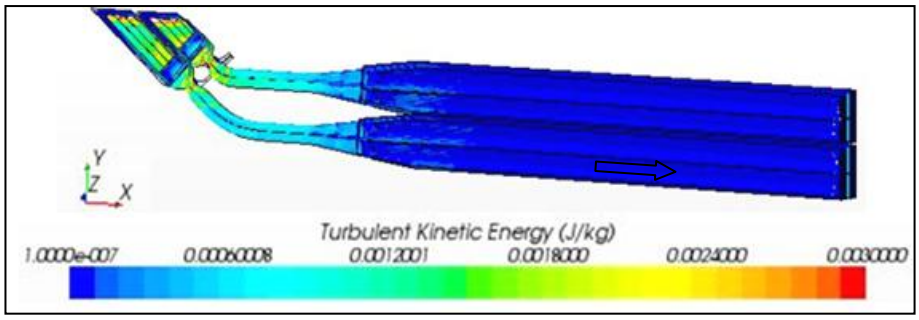

Figure 47 Distribution of turbulent kinetic energy in the model

8.1.6 Vorticity

Vorticity along the settling basin in Figure 48 shows the extent of swirling motion present in the settling basin. As expected from the development of TKE values, vorticity is significantly higher along the approach canal and at the inlet of the settling basin. Vorticity values are here as high as 2/s and reduces significantly along the stretch of the settling basin to 1.20×10^-5 /s. Vorticity close to the inlet of the basin is observed higher in the middle section than along the settling basin walls.

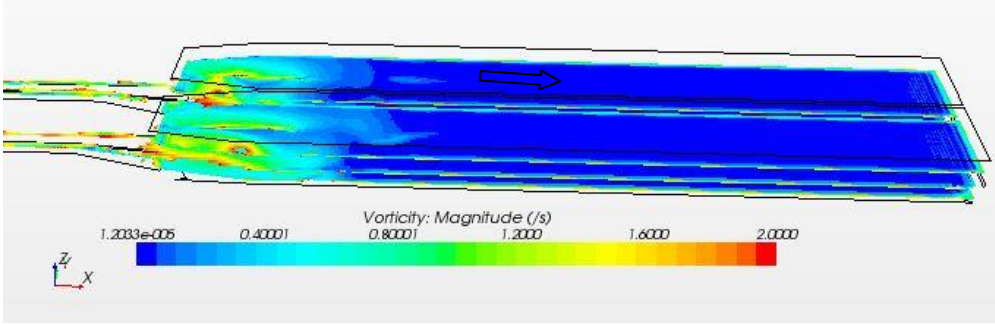

Figure 48 Vorticity along the settling basin

8.2 Results from measurements in the physical model

Results from the ADV measurements and the micro propeller measurements taken in the physical hydraulic model of LMM are presented below.

8.2.1 Velocity measurements along the intake

Velocity measurements along the intake were conducted with the help of micro propeller as explained in Chapter 6.3. Figure 49 shows the results from the velocity measurements for two different flows, which gives us an

understanding of the impact floods have on the intake hydraulics. The average monsoon flood has a prototype value equivalent to 287.0 m^3/s along the river and the average monsoon flow has a prototype value equivalent to 109.0 m^3/s in the river. The intake orifice numbers along the x-axis are the various intake openings numbered from 1-8 in the flow direction. Two sets of measurements have been taken during the average monsoon flood in order to analyze the uncertainties in the propeller measurements.

As can be seen from Figure 49 velocity measurements are significantly higher for the three upstream intakes during the average monsoon flow. The velocities at the two flows are rather similar for the rest of the downstream intakes. Data sets for the average monsoon flood conditions shows notably higher discrepancy for the upstream most intake, intake 1 and the downstream most intake, intake 6. Similarly, the flow appears to be more steady for data set numbered 1 than for data set 2 during similar flow conditions. Data set 1 has been used during the numerical simulation conducted in this work.

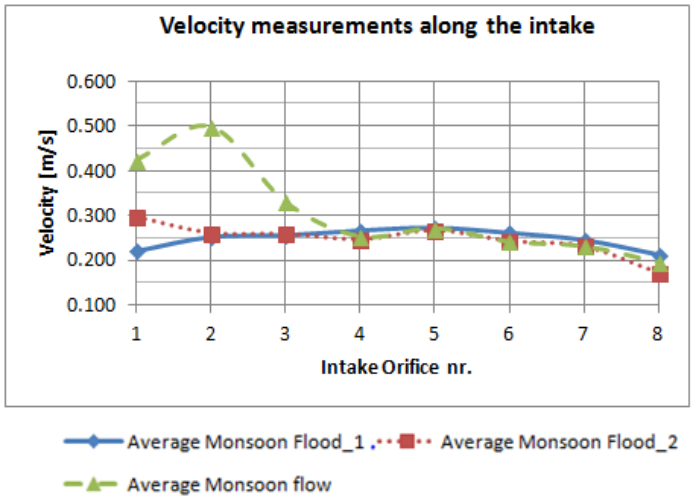

Figure 49 Velocity measurements along the intake

8.2.2 Velocity measurements along the gravel trap

Figure 50 illustrates the measurements conducted along various points at the gravel trap during the Average Monsoon Flood scenario. The points are measured at the intake as shown in Figure 34 in Chapter 6.2 where the points extend from the right bank to the left bank in the direction of flow and 1, 2 and 3 are located in the right gravel trap and 4, 5 and 6 in the left gravel trap.

According to figure 50 the trends in velocity variations is mostly similar for the propeller measurements and the ADV measurements along the gravel trap. However, propeller measurements seem to overestimate the velocity compared to the ADV measurements. Similarly, the velocities are higher in the left gravel trap compared to the right gravel trap with a decreasing trend from right to left bank along the flow direction. The velocity is highest at the right end of the left gravel trap and at the centre of the right gravel trap. The discrepancies between the two data sets are higher for the left gravel trap compared to the right gravel trap.

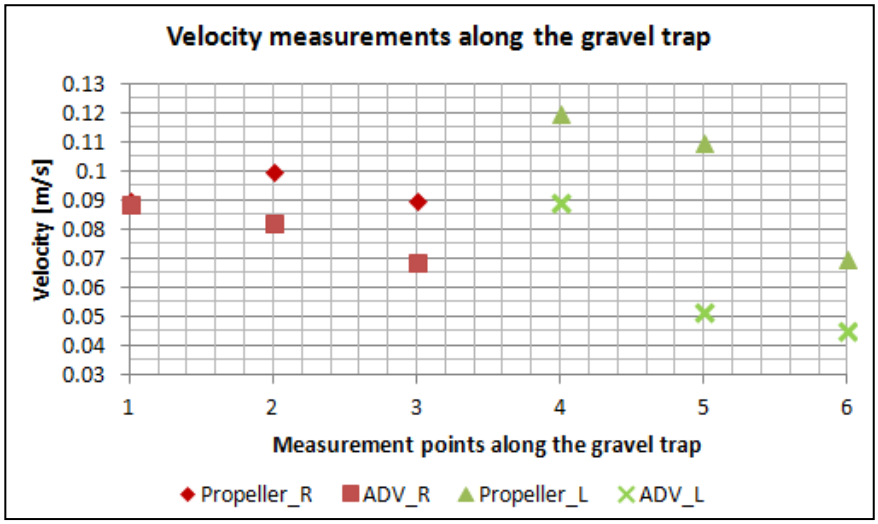

Figure 50 Velocity measurements along the gravel trap

8.2.3 Comparison of measurements and simulations

In this sub-chapter the numerically simulated results from the numerical hydraulic model of the headworks of LMM is compared to similar ADV measurements taken at the physical hydraulic model at Hydro Lab.

Velocity measurements and simulations along the settling basin

Figure 51, Figure 52, and Figure 53 below show the plots of simulated and measured velocities at various cross-sections along the settling basin.

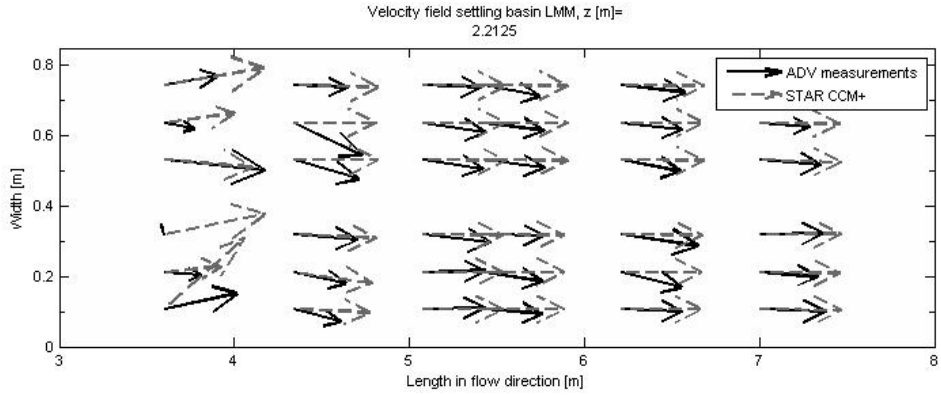

Figure 51 Comparison of velocity field close to the bottom of the settling basin

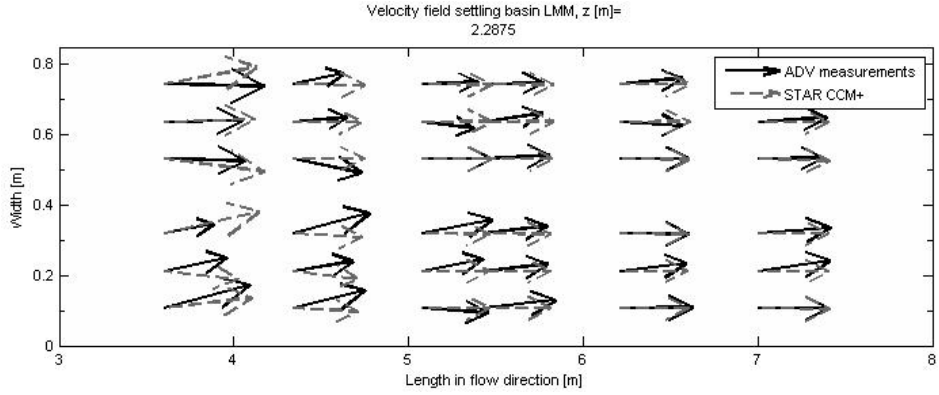

Figure 52 Comparison of velocity field along the middle plane section of the settling basin

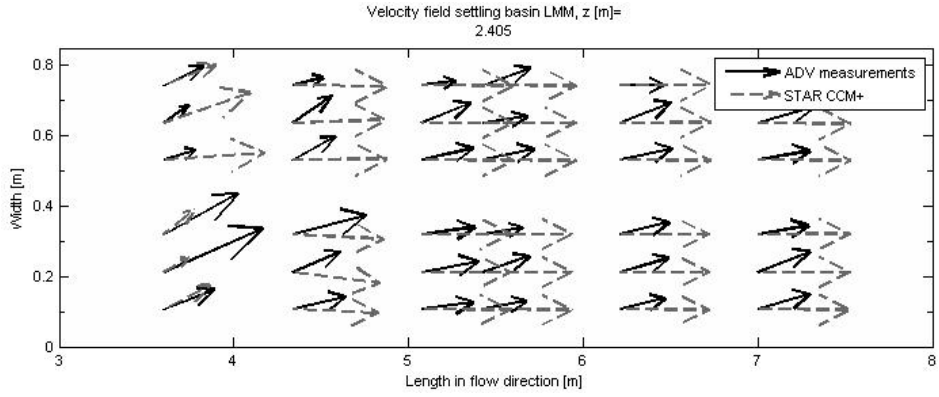

Figure 53 Comparison of velocity field close to the surface of the settling basin

ADV measurements along the plane section close to the bottom (z=2.21m) show skewed flows along the first five cross-sections up to a length of 7.00 m

fromFigure 51. The flow follows the flow direction close to the outlet of the settling basin. Relatively high velocities are measured at the inlet and the velocity magnitude seems to have gradually decreased from Cross-section 1(x≈4.00m) to Cross-section 3 (x≈5.20m). The velocities in the x-y plane seem to have stabilized from Cross-section 3. Though skewed the flows appear relatively symmetrical in the two basins.

The measured and the simulated flow is greatly turbulent at cross-section 1. The settling basin seems to perform well as the flow is calmer and relatively uniform compared to the desired flow along the flow direction. The approaching flow seems to be slightly more turbulent in the left basin and a higher approach velocity is observed from the plot in the left basin. Due to significant turbulence along Cross-section 1 the measured values seem unreliable as the flow seems to be stagnant at a width of 0.30 m from the right bank, whereas a significantly higher velocity is measured at the same point in Cross section 2 (x≈4.30m).

Simulated values along the plane close to the bottom have a slight deviation from the measured velocities. The flows here are uniform, symmetrical and follow the flow direction. The velocities seem to stabilize already at Cross-section 2 and the magnitude appears equivalent throughout the length of the settling basin from Cross-section 2.

From the tabulated values the simulations from Cross-section 2 and further along the settling basins along the various planes ranges mostly from 0.020 m/s to 0.040 m/s along the flow direction. The measured velocities in the lab fluctuate from 0.014m/s to 0.040m/s. Here, simulated flow values are along some points significantly higher than the measured values although both seem to give a similar range with a maximum prototype value of approximately 1.00 m/s.

Figure 52 shows that the flows along the mid-sections (z=2.28m) are relatively more calm, uniform and symmetrical than the two other plane sections. Although ADV measurements are slightly more skewed along Cross-section 2 relative to the flow direction the relative magnitude of the velocity between the two data sets seem to be equivalent already from the mentioned section. The flow here is more turbulent along the right settling basin as the flows here are slightly more skewed. Flow velocity from the ADV measurements seem to

have gradually stabilized from Cross-section 3. The deviation between the data sets is less giving more comparable results along the plane section.

The flow velocities appear to be more turbulent along the plane closest to the surface (z=2.24m) as seen in Figure 53. The simulated values are significantly higher along the settling basin. However, ADV values along Cross section 1 for the right basin are much higher than their respective simulated values. Based on the measured values the approach velocity in the right settling basin seems to be slightly more turbulent as skewed flows with a larger magnitude are observed here along Cross-section2. ADV measurements suggest a rather skewed flow following a similar direction in the two basins.

Figure 54 shows the velocity distribution in the y-z plane in the model along Cross-section 2. The velocity range here is notably small compared to the velocity in the plane direction and lies between 0.001 m/s to 0.006 m/s. The data sets show a random distribution for the simulated values and the measured values are found significantly different from the simulated ones. Circulations are observed from the measured values suggesting the presence of secondary currents. Similar distribution is shown in Appendix C for the remaining cross-sections. The circulations are observed along most of the Cross-sections.

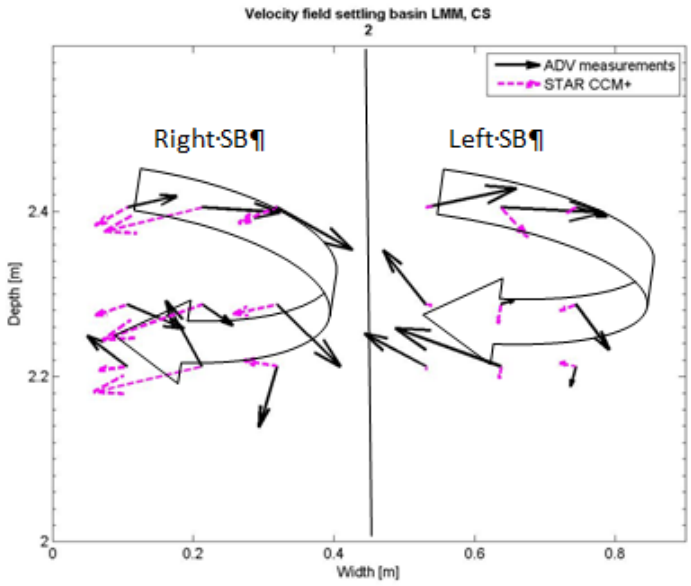

Figure 54 Velocity field settling basin LMM ,Cross-section 2

TKE along the settling basin

Figure 55 shows the development of turbulence along the settling basin based on the numerical simulation. ADV measurements are shown for comparison through circular nodes along the cross-sections in the same figure. Based on this figure the initial turbulence level at the inlet level shown in cross-section 1 is equivalent to the simulated TKE values. A slight deviation can be noticed at some points compared to the simulated values presented as the background of these nodes. The simulated TKE values decreases rapidly from cross-section 1 to 2 and stabilizes thereafter. More accurate results of the TKE values are shown through Figure 56.

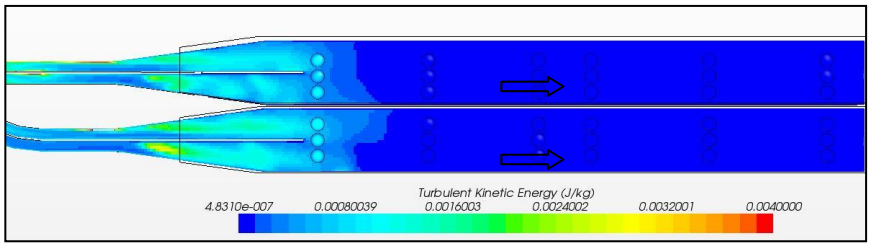

Figure 55 Comparison of TKE development along the settling basin

Figure 56 shows a graphical presentation of the development of TKE along the settling basin. A gradual decrease in the TKE values is observed for the ADV measurements whereas a rapid decrease is observed from Cross-section 1 to 2 for the simulated values. There is a decrease in 3 orders of magnitude from Cross-section 1 to 2 for the simulated values and the values appear constant at 1.00×10^-7. The discrepancy between the simulated values gets smaller along the settling basins as the measured values decreases gradually. The measured values decreases by one order of magnitude from Cross-section 1 to Cross-section 6 from 3.0×10^-4 to 1.00×10^-5. The turbulence in the left and the right settling basin appears symmetrical and uniform.

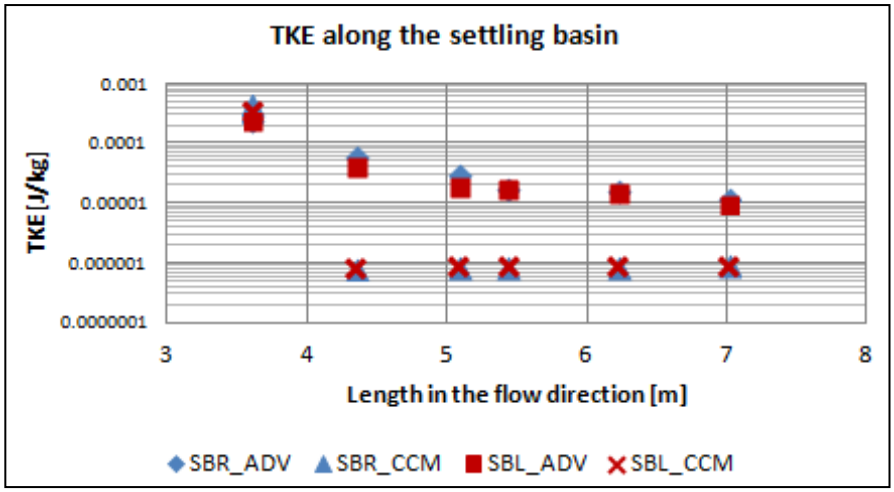

Figure 56 TKE along the settling basin

Figure 57 illustrates the TKE distribution along Cross-section 4. The measured TKE values here are one order of magnitude larger than the simulated values. The trend is opposite for the two data sets. The measured values shows a slight increase going from upwards in the positive z-direction from the bottom of the settling basin, whereas the simulated values show a slight decrease in TKE values along similar sections.

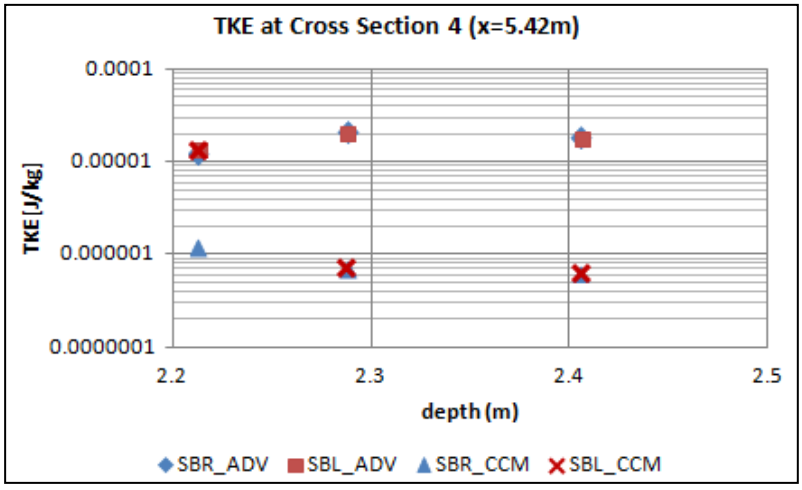

Figure 57 TKE at Cross-section 4

Velocity along the gravel trap

As high velocities were observed from, the numerical simulations at the inlet for the pressurized section along the gravel trap comparisons of similar sections have been made in Figure 58 . The circular nodes are values from ADV-measurements whereas the background shows the numerically simulated cross-section of the opening at gravel trap in the flow direction.

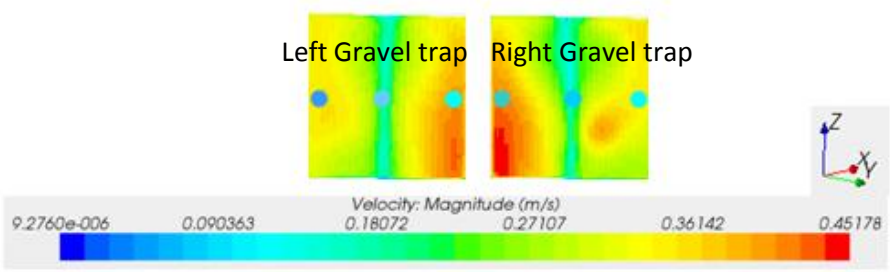

Figure 58 Velocity along the gravel trap

We observe that velocities at the centre point are quite similar, however simulated velocities are significantly higher compared to the measured ones at the inlet walls in Figure 58.

Turbulent Kinetic Energy (TKE) along the gravel trap

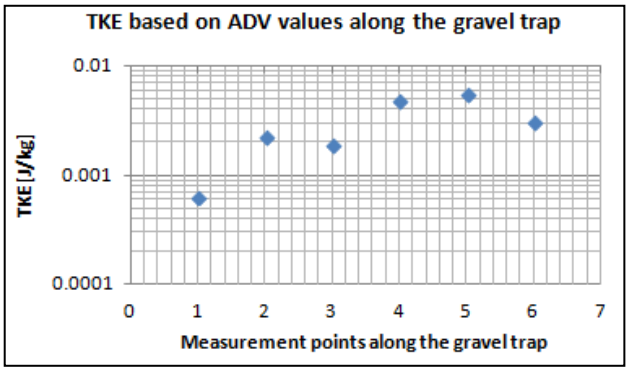

Figure 59 TKE based on ADV measurements along the gravel trap

Based on Figure 59 the measured values show a significantly high level of turbulence along the gravel trap with a maximum range of 0.003 J/kg. Turbulence is also observed higher along the left gravel trap. TKE values here

are in the left gravel trap significantly larger than the ones simulated for Cross-section 1 shown in Figure 59Figure 47. The TKE values for the measured data are highest at the centre of each gravel trap and turbulence level along the left settling basin is observed to be notably higher than the right gravel trap, which is similar to the trend seen from the simulation results.

8.3 Vorticity in the numerical simulation

Based on Figure 60 the vorticity decreases gradually until Cross-section 3 (x≈5.20m) and then starts to increase at a smaller rate until Cross-section 6 (x≈7.00m) suggesting higher level of circulation close to the outlet and near the inlet.

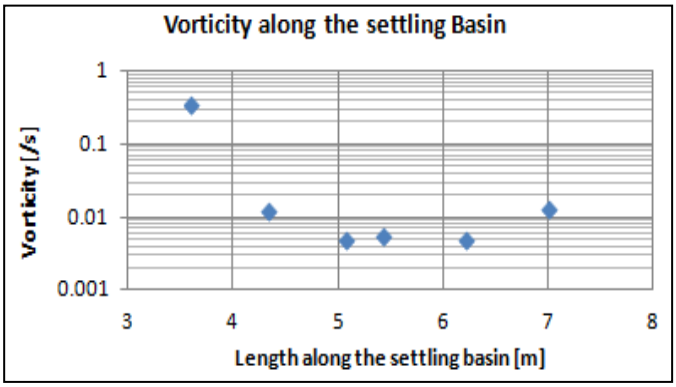

Figure 60 Simulation of vorticity along the settling basin

Figure 61 gives an overview of the development of vorticity at various depths along the two settling basins at Cross-section 1 , 4 and 6. Circulation formation is larger along the right basin (R) for Cross-section 1. The vorticity along the right basin is less at Cross-section 4 compared to the left basin (L). Vorticity development is relatively equivalent along Cross-section 6 as can be seen from the above figure. Vorticity development along Cross-section 6 and Cross-section 4 show a similar trend along the depth of the settling basin whereas vorticity decreases with depth along Cross-section 1.

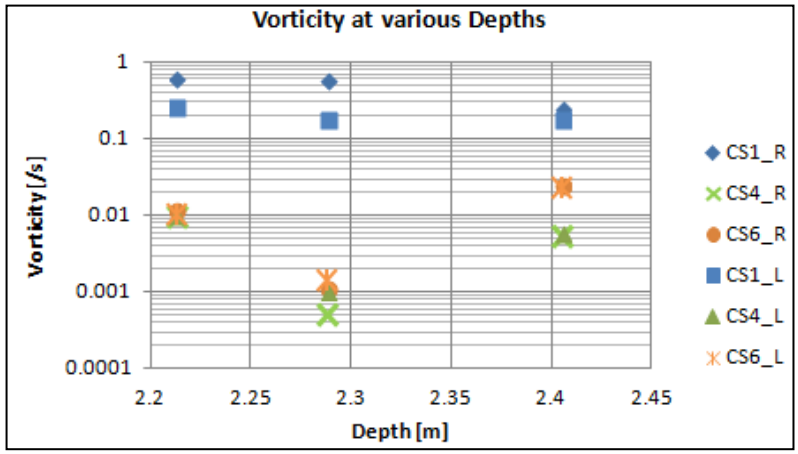

Figure 61 Simulated vorticity at various depths

9 Discussion

This chapter briefly evaluates the study conducted at the physical hydraulic model in Chapter 8 and analyzes the results presented in Chapter 9. Furthermore, uncertainties in the results and measurements are also discussed under each sub-chapter.

9.1 Physical Hydraulic Model studies of Headworks

Based on experiences gained from the case studies conducted and the Physical Hydraulic Model study of the LMM HPP the design of headworks is often a compromise between the various performance standards mentioned in Chapter 3.1.1 and the economic viability of the project. In river conditions with steep, sediment-loaded rivers, it is extremely important to focus on the design of settling basins while designing the overall headworks.

Existing power plants such as Khudi HPP discussed in Appendix A have been subjected to clogging at the intake due to poor sediment management. The ability of headworks to separate bed load before the intake or upstream of the settling basins ensures that the abstracted water to the settling basins is free of bed load. Separation of sediments and thereby a controlled bed at the intake is obtained by the use of bed load sluices as in the case of Khudi HPP and LMM HPP or undersluices as used in Kabeli 'A' HPP .

Flushing arrangements and operations of the flushing gates such as the bed load sluice gate and the gravel trap flushing gate also need to be carefully considered as these will have an impact on the hydraulics at and along the intake. Lack of proper flushing head leads to reduced flushing efficiency and thereby an increase in bed level in front of the intake causing larger amount of sediment to be transported along the intake. A decrease in the efficiency of the settling basin is then followed by passage of sediments through the conveyance system causing erosion along the conveyance system and of the mechanical components.

Passage of flood is also one of the major design considerations, however, this rarely seems to be a problem in the reviewed projects. However, the design of stilling basin needs to be considered for the proper dissipation of energy especially during higher floods, as studied and observed for the PHM of Kabeli

'A' and LMM HPP. Furthermore, downstream areas that are susceptible to erosion need to be protected with the use of riprap.

Intake hydraulics as seen for all three cases greatly affects the transport of sediments near and along the intake. Use of river training structures to guide the flow by securing the impact of an outer curvature along the intake orifices both helps in diverting the sediments away from the intake and ensuring a reasonably uniform flow towards the intake as discussed in Chapter 3.1.1. Securing good hydraulics at the intake along with a proper floating debris passage also aids in handling of trash and floating debris. Similarly, the use of slots and divide walls to reduce the size of eddies formed in and along the intake structures helps to secure the desired hydraulics at the intake structures. Weir crest increment is also in some cases an effective way to reduce the velocities in front of the intake such that sediment transport, especially of large boulders that can create damages to the intake structure and disrupt the intake hydraulics is significantly reduced.

A highly sediment loaded river in most cases requires both a bed load sluice followed by a gravel trap and settling basins for proper sediment exclusion as designed for the LMM HPP and Khudi HPP. As seen from these case studies the PHM study is often used to improve the design of the settling basin structures to ensure flow condtions as discussed in Chapter 3.1.3. The size and shape of the settling basins needs to be designed in such a way that even flow distribution for trapping of suspended sediments within the settling basins along with efficient removal of deposits is secured. Symmetric layout of the settling basins along with smooth transitions and use of divide walls along the approach canal and inlet transition as theoretically explained in Chapter 3.1.3 was observed to be an effective way of securing symmetrical uniform flow along the settling basins. Use of intermittent flushing is often a good compromise between ensuring regularity in power generation capacity of the plant and securing proper management of sediment. Slotted pipes and the S4 system have been recommended for the flushing arrangements of LMM HPP.

River hydraulics and sediment study is a complex process and specially in a country such as Nepal where both the available data quantity and their quality is questionable, analytical calculations are often not enough to secure a functional headworks design. Thus, it is often difficult to foresee and

understand the functional aspect of the intake without a physical hydraulic model study. Despite the scale effects discussed in Chapter 3.2 physical hydraulic model study helps in studying both intake hydraulics and sediment transport tendencies along the intake. Problems can then be identified and improvements suggested through tests on the model to ensure a functional design of headworks.

9.2 Measurements on the Physical Hydraulic Model

Based on the comparisons made for the two data sets measured at the intake for the Average Monsoon Flood condition it can be concluded that micro propeller measurements are of good quality. The accuracy of the data is difficult to validate as only micro propeller was used to measure along the intake. According to the specifications from the company that designed the propeller the instrument has an uncertainty range of 3% of the measured value. The variations at inlet 1 can be caused by standing waves and turbulence observed near the intake above the bed load hopper when the measurement was taken. Similarly, the variations at inlet 8 could be due to a difference in regulation of the flap gate used for the passage of trash and debris while the measurements were taken. The presence of a gate disrupts the flow and back flows might create variations in the velocity fields near inlet 8. Discrepancies in the two flow conditions presented are the result of varying operations of bed load sluice gate and the trash passage gate.

Based on the velocity measurements in the gravel trap, Micro propeller seems to overestimate the velocity compared to the ADV measurements along the similar stretch. The propeller averages the velocity measured during an interval of 10.0 s such that the velocity ranges become higher during this interval. The ADV measurements are point measurements at an interval of 1.00 s and records 50 data per measurements including the rapid fluctuations in velocity. ADV measurements are thus more accurate point measurements whereas the Micro propeller can be used to estimate the upper ranges of velocity fields in the flow. The velocities were also observed higher in the left gravel trap compared to the right gravel trap which is due to a shorter distance from the intake orifice to the gravel trap in the left gravel trap. The discrepancies from the propeller data are consequently higher. The decreasing trend from the right bank to the left bank in each of the gravel traps is caused by a slight head difference in the flow direction along the intake orifices.

9.3 Comparison of simulated results and measurements

In order to verify the use of numerical modeling in the field of hydropower as an alternative to physical hydraulic modeling similar flow conditions were adopted at the inlet for the average monsoon flood scenario to replicate the flows along the settling basins. Based on the results shown in Figure 52 the plane section along the centre of the settling basin is able to reproduce similar results from the simulations as the measured ADV values. The plane section closest to the surface shows the most deviation from the measured data which can be defined by the errors caused by the use of Volume of Fluid (VOF) model in the simulations. On using the VOF model Star CCM also takes into account the velocities in the atmosphere above the free flow along the basins.

In addition to this, ADV measurements are also likely to have been influenced by the impacts of wind velocity as slight formation of waves was visible along the surface despite the attempts to protect the flow along the basins by covering them with wooden planks. The plane section closest to the bottom is most likely to be affected by the roughness and shear stress development at the bottom as the numerical model is not calibrated with measurements from the physical model for such parameters causing discrepancies in the simulated data relative to the measured flow data.

Based on the ADV measurements, the secondary currents, as shown in Figure 54 for Cross-section 2, form a slight circulation in the clockwise direction. The numerical model seems to be incapable of reproducing these trends. The deviation here is governed by the initial conditions selected. Changes in the parameters of the physics continua will probably give a different outcome. Velocities are observed higher near the settling basin walls, which might be due to the effects of wall shear stress.

Reynolds number, used to estimate the turbulence level in the water only takes into consideration the hydraulic radius of the settling basin and the velocity of the flow. The Reynolds number is similar for almost all the cross-sections and is equivalent to 30 000 as the area and the discharge is equal. The Reynolds value only suggests that the flow is turbulent along the settling basins. TKE is, therefore, used to further analyze the degree of turbulence in the water and how the turbulent regime changes along the settling basin's length. The simulated TKE values are significantly low compared to the measured values.

The TKE as expected decreases along the stretch of the settling basin and similar trends are also observed for the two basins. The selection of turbulence models in the numerical simulation affects the simulation output. A different turbulence model is therefore probably suited for this simulation. Changes in turbulence intensity were also analyzed without any significant effects in the results. Other parameters such as the turbulence viscosity ratio can also be altered for further analysis.

TKE has also been calculated for measurements along the gravel trap. The TKE is dependent on velocity fluctuation and the TKE values show similar trend as the velocity measurements along the ADV. Turbulence level is higher along the left gravel trap as higher velocities were observed here and turbulence level at both the gravel trap is greatest along the centre.

Turbulence level in the numerical model was further analyzed by extracting the simulated vorticity values. Vorticity as the TKE value is greatest along Cross-section 1. A gradual decrease in vorticity as expected occurs until Cross-section 3 as the impact from the inlet transition decreases along this stretch. A slight increase in vorticity occurs from Cross-section 4 to Cross-section 6 which is assumed to be due to the impact from the outlet on the flow inside the settling basins. Vorticity seems to be less prominent along the centre plane section of the settling basin which also explains the results from the velocity distributions simulated along this plane, which were similar to those of the measured ones.

10 Conclusion

Headworks design in steep, sediment-loaded rivers such as the Marsyangdi River is deemed difficult. In addition to the challenging topography and seasonal variation in sediment load and the river flow, the lack of reliable sediment and hydrology data creates difficulty in designing the headworks of any water resources project. Operational reliability of the initial design is often questioned and a physical hydraulic model becomes a necessary tool to ensure successful operation.

Experience from the case studies of physical hydraulic model studies has shown that study of sediment transport patterns and capacity is complex. Passage of sediments and bed control during flood periods with highly concentrated sediments and discharge has been the major challenge in LMM model study. Design of an optimal bed load handling facility and settling basin for dealing with sediments is, therefore, very important to handle the sediments in a proper way without affecting the regularity in power generation of the power plant.

Intake hydraulics is seen to be a governing factor in the design and transport of sediments along the intake. Through dye tests, it has been shown that final conceptual design has improved hydraulics in front of the intake. Vortices/eddies in front of the intakes and along the settling basins have been reduced and a uniform, symmetrical flow has been achieved along the settling basins by the modifications made in the initial design through various model tests. Secondary currents in the flow determine the turbulence level in the flow, which is a governing factor for the settling of sediments in the basins.

Velocity measurements along the gravel trap and settling basins have shown that the desired velocity level along the basins has been achieved with a maximum velocity magnitude along the basin of approximately 1.00 m/s prototype value. Further evaluations of turbulent kinetic energy have shown significant decrease of turbulence level along the settling basin.

The use of numerical model has to a large extent been successfully able to replicate the hydraulics in the modeled headworks of LMM HPP. The velocity

range is comparable to the measured values in the laboratory. Flow fields close to the surface and the bottom vary significantly along the first few cross-sections. However, the velocities are similar close to the outlet. Flow fields in the middle of the basins are the ones that are most similar to the ADV measurements.

Secondary currents along with the TKE have not been reproduced properly in the numerical model. TKE for the first cross-section close to the inlet of the basin is similar to the measured values in the lab. However, no significant trends in TKE values can be observed between the simulated values and the measured values otherwise along the length of the basin.

Numerical models have required boundary conditions determined from the physical hydraulic model and the results have been validated against physical measurements from the lab. Thus, it is recommended to use numerical model study in combination with physical hydraulic model study. The numerical model requires an initial validation of the replicated flows against the measured flows from the laboratory. Then the validated numerical model can be used to predict further effects of changes in the headworks design and to optimize the conceptual design.

11 Further work and Recommendations

The effects of secondary currents should be considered in further detail when designing the settling basins. This study has not been able to establish a direct relationship between the TKE values and the design of the settling basins as prototype values are neither simulated nor measured. The ratio of TKE values and the average shear stress at a particular point should be equal in both the model and the prototype. Due to time constraints, the author has not been able to establish this relationship. Thus, the prototype equivalent TKE values along the settling basins, which could have been used to compare against values from other research projects, have not been calculated and is recommended for further work.

Numerical modeling in Star CCM+ is a very comprehensive process as the setup is based on parameters and algorithms selected as the continuum of the model explained in Chapter 7.2. Due to the constraint in time and inexperience of the author the parameters selected might not have been optimal. Detailed parameter sensitivity analysis incorporating the various turbulence models, finer grid sizes, changes in turbulence viscosity and impacts of relaxation factors needs also to be conducted for further study of the numerical model.

The Numerical Hydraulic Model conducted in this work is limited to the study of intake hydraulics. Further study could focus on the study of sediment transport along the headworks incorporating all the headworks components to gain a better understanding of the headworks performance using numerical models as sediment measurements have also been conducted at the headworks area.

Bibliography

ADAPCO, C. 2012. User Guide Star CCM+ Version 7.04.006. *In:* ADAPCO, C. (ed.).

BALZEK, J. 2005. *Computational Fluid Dynamics: Principles and Applications,* London, Elsevier Ltd.

BANERJEE, S. G., SINGH, A. & SAMAD, H. 2011. Power and People : The benifits of renewable energy in Nepal Washington DC: The World Bank.

BOGATI, P. R. 2012. Physical Hydraulic Model study of the headworks of Kabeli 'A' HEP-Final report. Pulchowk,Lalitpur: Hydrolab Pvt. Ltd.

BPC, B. P. C. 2011. *Lower Manang Marsyangdi* [Online]. Nepal: BPC. Available: http://www.bpc.com.np/index.php?option=com_page&task=details&id=27 [Accessed 07.02 2013].

CHANSON, H. 2004. *The Hydraulics of Open Channel flow: An introduction,* Oxford, Elsevier Ltd. .

COURANT, R., FRIEDRICHS, K. & LEWY, H. 1956. On the partial difference equations of mathematical physics. New York: AEC

GARCÍA, C. M., CANTERO, M. I., NIÑO, Y. & GARCÍA, M. H. 2005. Turbulence Measurements with Acoustic Doppler Velocimeters. *Jorunal of Hydraulic engineering*, 19.

GUTTORMSEN, O. 2006. *Vannkraftverk og vassdragsteknikk II,* Trondheim, Tapir akademisk forlag.

HASAAS, Å. 2012. *Verifisering av inntakshydraulikk i grunt inntaksmagasin for småkraftverk med bruk av CFD-verktøy.* Masters, NTNU.

JACOBSEN, T. 1997. *Sediment problems in reservoirs-Control of sediment deposits.* Doctorate, NTNU.

JENNSEN, L., TESAKER, E., STEINAR, L. & HUBER, D. 2006. Inntakshåndboken. *En rettledning for planelgging og utforming av inntak til småkraftverk.* Oslo: NVE

NTNU.

KETTNER, F. 2010. *Numerical modelling of flow over spillways.* Masters, NTNU.

LYSNE, D. K. 1982. Laws of Similitude for Model studies.

LYSNE , D. K., GLOVER, B., STØLE, H. & TESAKER, E. 2003. *Hydraulic Design* Trondheim, NTNU Department of Hydraulic and Environmental Engineering

NAI, C. C. 2004. Project completion Report on the Kali Gandaki "A" Hydroelectric Project in Nepal.

NIELSEN, L. E. & RETTEDAL, B. 2012. *Different Aspects of Flushing of Hydropower Intakes.* Masters, NTNU.

OSLEN, N. R. B. 2011. *Numerical Modelling and Hydraulics,* Trondheim.

SHRESTHA, H. S. 2012. *Sedimentation and Sediment Handling in Himalayan Reservoirs.* Doctorate, NTNU.

SHRESTHA, U. & BOGATI, P. R. 2012. Physical Hydraulic Model study of the Headworks of Lower Manang Marsyangdi HEP. Kathmandu, Nepal.

SHRESTHA, U., PRASAD, P. P. & BISHWAKARMA, M. B. 2008. Hydraulic Model study of the headworks of khudi hydropower project. Pulchowk, Lalitpur: Hydrolab Pvt. Ltd.

STØLE, H. 1993. *Withdrawal of water from Himalayan Rivers.* Doctorate PhD, NTNU.

VERSTEEG, H. K. & MALALASEKERA, W. 2007. *An Introduction to Computational Fluid Dynamics,* Edinburgh, Pearson Education Limited.

Appendix A Case studies of headworks design of physical hydraulic models (PHM)

This chapter deals with the study of headworks arrangements of two physical hydraulic model studies performed at the hydraulic laboratory of Nepal, Hydro Lab. Physical model studies of two projects are presented on the basis of the report prepared by Hydro Lab. Kabeli 'A' HPP has been studied for development whereas Khudi HPP is an existing plant, which is under operation. The study identifies problems in the design phase. Cases are furthermore, compared and evaluated with respect to the modified arrangements based on the model study conducted at the laboratory and the theoretical background for headworks arrangements presented earlier in Chapter3.

Kabeli A HPP

Kabeli A HPP is a 38 MW daily peaking reservoir project studied for development. The project is situated along the Kabeli River that flows along the border between Taplejung and Panchthar Districts, Mechi zone in the eastern region of Nepal. The catchment area at the proposed headworks site shown in Figure 62 is 864km^2 with a 40 percentile flow as the design discharge at 37.73 m^3/s and a gross head of 116.8 m.

Figure 62 Headworks site of Kabeli'A' HPP(Bogati, 2012)

In order to evaluate the general hydraulic performance of the initial design as provided by the client a physical hydraulic model was developed at Hydro Lab

in a scale ratio of 1:50. The study is based on the report prepared by Bogati (2012).

Initial arrangement vs the Final arrangement

The performance of the headworks has been assessed with respect to the performance standards discussed in Chapter 3. This case study presents the problems that were identified in the initial design and the suggested modifications for the final design along with their evaluations. The structural design of the initial arrangement has not been further discussed in this section as the case study focuses on the functionalities of the design. Figure 63 illustrates the initial arrangement of headworks as provided by the client for further study.

Figure 63 Kabeli A Headworks of the initial design (Bogati, 2012)

Withdrawal of water

The plant is designed for the withdrawal of 120% of design discharge (45.3m^3/s) throughout the year. Several tests were performed on the model at different flows. Based on these tests it was concluded that the submergence of the side intake adopted in the design was critical as small drawdown in water level in front of the intake caused air entrainment through headrace tunnel. Vortices were observed in front of the intake causing the entrainment of air. Figure 64 shows the initial arrangement of the intake with the intake orifices (8.00m× 5.50m high with sill level at 564.7 masl wide numbered as (1).

Operation level was increased by the client by 2.00 m in order to get more submergence of the intake. The model study consultant in agreement with the client then made the following modifications intake shape, size and invert level was altered for sufficient submergence. It was made wider with two identical intake orifices (12.0 m wide × 4.30m high with sill level at 566.7 masl) as shown in the final arrangement of the headworks by figure...

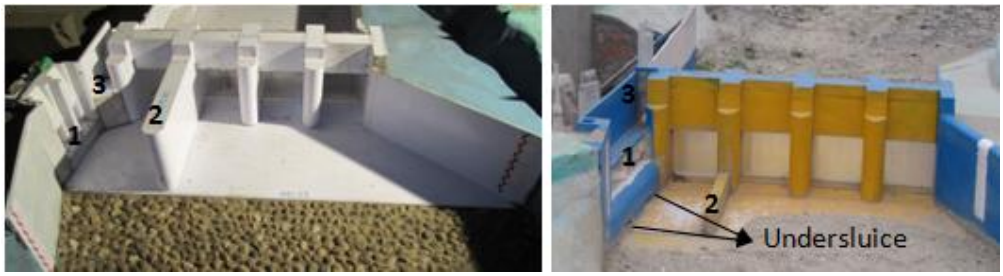

Figure 64 Initial (Left) vs Final (right) intake design Kabeli 'A'

The designed intake divide wall in the initial design numbered (2) in figure26 created turbulence in front of the intake causing significant bed load suspension in front of the barrage. The intake divide (22.5 m long ×2.00 m width×10.5 m high) wall was studied for optimization and placed upstream of the right pier of the barrage gate closest to the intake to improve intake hydraulics and bed control in front of the intake.

Different alternatives were tested for the size of the intake divide wall and a 22.5m long × 4m high divide wall was selected. The adopted divided wall had no effect on the intake while maintaining the water level at MDL, lower sediment deposition was observed between the intake and divide wall and rotational flows had negligible impact on the flow.

- ***Passage of floods***

The initial design is assessed for the safe passage of hazardous floods through gates with proper energy dissipation within the stilling basin.

The originally designed spillway as shown in Figure 65 was observed to be capable of passing all floods tested on the model. The 100-year flood is 1920m^3/s and the Probable Maximum Flood (PMF) is the 1000-year flood at 2750 m^3/s. The average annual flow at the dam site for Kabeli 'A' HPP is 51.75 m^3/s.

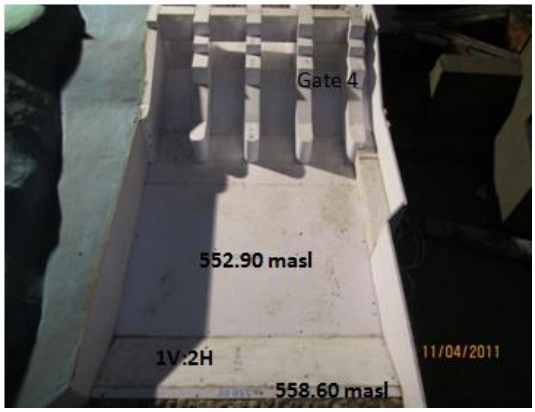

Figure 65 Initial design of the stilling Basin at Kabeli'A' HPP(Bogati, 2012)

As the client had increased the operation levels the stilling basin of the conceptual design prepared by the model study consultant did not meet the performance standards required especially during dry season when the water level was maintained at the Full Supply Level (FSL) at 577.3 masl in the reservoir and operating only one gate. Stilling basin designs were after several trials altered increasing the basin width and length to 61.0 and 50.35 m respectively with a lowering of the invert level by two meter. The level of the basin was set to 558.10 masl maintaining a 1V:2H slope at the upstream face as illustrated in figure 27.

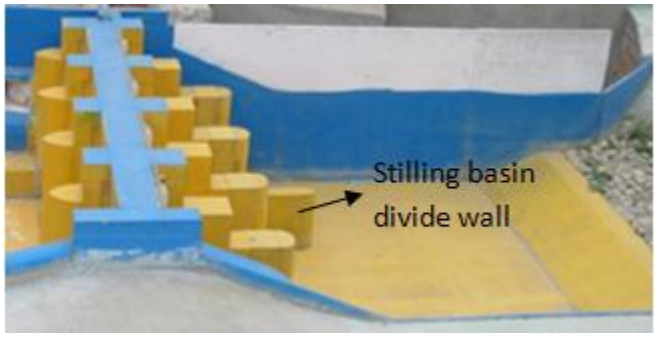

Figure 66 Final design of the stilling basin at Kabeli 'A' HPP

Rotational flow in the stilling basin was observed when operating the intake undersluice and the gate closest to the intake, Gate 4, shown in Figure 66. Several alternatives of the stilling basin divide wall were tested to improve the hydraulics. A 10.0 m long × 2.0 m thick × 8.0 m high of the stilling basin divide wall was selected in the final design shown in figure 28 which helped to reduce

the rotational flows in the basin such that they became insignificant. The performance of stilling basin was found satisfactory for all flood hydrographs simulated on the model with the maximum of 1000 years flood.

- ***Passage of ice, trash and floating debris***

Vortices that were observed in front of the intake also led to the transportation of floating debris into the conveyance system. Accumulation of floating debris along with rotational flow was seen in front of the intake and the gate closest to it and it was deduced that the capacity of the floating debris spillway was low (numbered (3) in Figure 64. Floating debris passage (3.0 m wide × 51.9 m long) is located above the intake and a control gate (3.0 m ×4.0 m) is located beside the barrage pier.

Based on the tests of some selected flows problems with the passage of floating debris was observed for flood hydrographs with up to 50 years of return period. Only debris that came towards the intake was extracted by the floating debris passage while the remaining was observed to be accumulated in front of the barrage gates. Based on this, modifications were made to the floating debris passage and the intake by lowering it down to a meter in order to improve debris passage and increase intake submergence. Modifications were made without testing on the model.

- ***Bed Control at the intake***

The initial design of the headworks is meant to develop a storage of 0.44 Mill.m^3 of water for daily peaking without depleting the reservoirs storage capacity due to sediment loads.

In order to ensure bed control in front of the intake a scenario test was performed to estimate possible bed deposition level during the worst possible conditions at the headworks. Sediment load was filled with a clearance level of half a meter to the Minimum Drawdown Level (MDL). This reduced the storage of the reservoir by 0.04 mill m^3 while maintain the MDL in the reservoir. Flushing with a discharge of 1 year flood (277m^3/s) the live storage was recovered by 0.017 mill m^3. Deposition was nonetheless high in front of the intake leading to excessive sediment passage along the intake and towards the settling basins.

Two intake undersluice openings (4.0m × 1.0m) with sill level increased at 561.5 masl were placed beneath the intake orifices Figure 64 and are connected to a pressurized culvert (2.0m ×3.0m) up to the flushing gate followed by free flow type culvert/chamber (3.0m × 6.55m) downstream of the gate.

Worst possible scenario case was developed as for the initial arrangement to assure bed control in front of the intake. Eddies were also observed in front of the undersluice gates close to the pier beside the floating debris passage. Flushing efficiency could be increased by opening the flushing gates for a certain period so that delta formation upstream the barrage could be flushed by the available river flow at the time of flushing. It was found hard to flush deposits from higher floods with the usage of lower floods/flows, which led to the formation of huge deltas and deep channelization within the reservoir area due to the lack of undersluice beneath the intake.

Based on the observations flushing has been recommended at least once during the wet season during the peak period of each flood. It is suspected that more frequent flushing might be required based on the deposition and sediment load in the river inflow. For an effective operation of the plant it is furthermore suggested that flood and sediment monitoring and early warning system be installed within the reservoir and at suitable location upstream of the reservoir.

Performance of the intake undersluice and thereby the bed control in front of the intake was found satisfactory. The final design is intended to ensure safe passage of sediments downstream with minimum impact to the natural flow of the river.

- ***Exclusion of suspended sediments***

The settling basins are designed to trap 90% of the suspended particles with size larger than 0.2mm. Based on the dye test skewed, turbulent flows were observed at the inlet transition of the settling basins.

The settling basin approach tunnel alignment and transition sections were also modified. Alignment of two identical approach tunnels was changed by introducing only one bend instead of two bends, which provided a longer transition section to the settling basins, as shown in Figure 67.

Figure 67 Final design of the approach tunnels for the PHM of kabeli 'A' HPP

Sizes of the approach tunnels (3.2m ×3.2m) and the barrage gates were left unchanged. Settling basins were designed with double hoppers, increased transition length and slotted weirs at the outlet followed by outlet transition section/tunnels transporting water from each of the settling basin to a common headrace tunnel. Figure 68 shows the final arrangements made on the model for this project.

Figure 68 Final design settling basin Kabeli 'A' HPP

Though skewed flows were observed in the approach tunnel due to unsymmetrical geometry of the orifices and differing approach flow conditions upstream the intake, the hydraulic performance the settling basins were improved with calm and uniform flow conditions from the start of the uniform section in the basin. Problems were observed concerning sediment deposition within the pressurized transition section, which would be difficult to flush and modifications were therefore required for further improvement of the hydraulic performance.

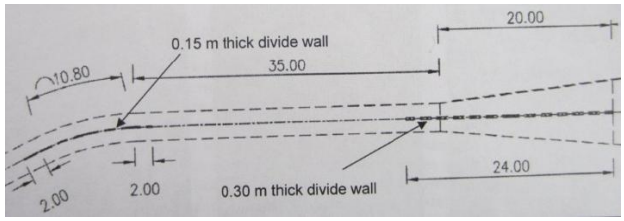

Figure 69 Modifications at the approach tunnel and inlet transition of the settling basin(Bogati, 2012)

Acceptable improvement was made when modifications were made to the upstream (left) settling basin (Figure 69) to reduce the uneven flow in the approach culvert and thereby improve the hydraulic performance. The straight portion of the approach tunnel was increased, a divide wall was introduced at the centre approach tunnel bend extend it by 2.00m both upstream and downstream. Divide wall was also placed at the expanded transition section and extended 4.00m upstream inside the approach tunnel. Finally, the pressurized portion of the expanded transition section was reduced by 10.0m.Symmetrical and uniform flow conditions were then observed in the approach tunnel and the settling basin for various discharges that were tested.

Thus, the final arrangement shown in Figure 70 was adopted for further study and development as it provided satisfactory hydraulic performance and met all the performance standards set for functional headworks.

Figure 70 Final arrangement Kabeli 'A' HPP

Flushing of settled sediments

The S4 system presented in chapter 3.2.4 is planned to be used for flushing of settled sediments from the settling basin. Additional 20% of the design discharge abstracted from the river through the intake is to be used for flushing of settled sediments. Physical model study does not include the study of the S4 system and flushing of the basins and has not been assessed further for this study.

Khudi HPP

Khudi HPP is a small run-of-river HPP with an installed capacity of 4MW and a gross head of 103m. The project is located in Lamjung District in Midwestern region of Nepal. The project was commissioned on December 30, 2006. The catchment area at the headworks site is located at the confluence of the Marsyangdi River and is about 127km^2. The design flow is at 4.90 m^3/s whereas the mean annual flow in the river is about 9.80 m^3/s and the mean dry season flow is approximately 2.80 m^3/s. Figure 71 gives an overview of the headworks site at Khudi HPP.

Figure 71 Headworks site of Khudi HPP (Shrestha et al., 2008)

In order to evaluate the general hydraulic performance of the existing headworks design as provided by the client a physical hydraulic model was developed at Hydro Lab in a scale ratio of 1:30.

Already during the first monsoon after the plant came to operation in 2006 the plant suffered from cloggage of the intake and the bed load sluice several times. The client decided to carry out modifications of headworks in the existing model at Hydro Lab for the improvement of the headworks performance. The main objective of the PHM as stated in the final report by Hydro Lab are as follows (Shrestha et al., 2008):

1. Investigation of the causes of clogging of the flushing units and the intake hopper.
2. Provide modification for improved performance of the headworks.
3. Conduct a study of the hydraulics and sediment transport patterns before and after the modification.

4. Check the flushing ability of the bed load sluice.
5. Verify the abstraction of design discharge through the intake.
6. Recommend operational procedures for improved operation and maintenance of the plant.

The salient features of the initial arrangement have been presented in Appendix… and have not been further discussed in this section as it is the functionalities the case study focuses on and not on the structural design itself. The case study is specially relevant for understanding methods of sediment handling and removal with respect to bed control and sediment passage at the intake. The left and the right riverbank are differentiated while looking downstream along the flow direction.

The initial arrangement

Figure 72 PHM of the headworks of Khud HPP (Shrestha et al., 2008)

Figure 72 shows the PHM of the initial arrangement of the headworks area of Khudi HPP. Clogging of the bed load flushing culvert was experienced at four different occasions during the first monsoon operation of the plant. The clogging of the bed load sluice and bed load hopper eventually led to an increase in bed level in front of the semi-frontal intake due to sediment entry into the gravel traps causing blockage of the entire intake. Very large logs and boulders up to 0.62m was reported to be removed manually from the gravel trap area (Shrestha et al., 2008).

Several flows were tested on the model; both moderate flows and floods. The bed load characteristics and the flow patterns were studied in order to identify the factors responsible for intake blockage. Based on the tests performed nearly 2/3 of the bed load sluice was observed to be under pressurization during an average monsoon flood (80.0 m^3/s) even in the absence of flow contribution from the connected gravel trap. The pressurization length varied with the extent of sediment concentration in the sluice. The pressurized flow along the bed load sluice decreased the flow velocity causing sediment deposition in the sluiceway.

Similarly, deposition was observed downstream of the bed load sluice that extended upwards, suggesting insufficient flushing head in the sluice. Pressurized flow in the bed load sluice was also enhanced by the entry of big boulders in the sluice. Entry of smaller boulders and further interlocking also induced further deposition. For a particular flow the performance of the bed load decreased with an increase in sediment concentration it is, therefore, also suggested that the bed load sluice blockage might also be a result of unexpected amount of sediment inflow during flood.

Downstream river morphology also seemed to have an impact on the flushing efficiency as there was no elevation drop in the river up to nearly a stretch of about 20m from the bed load sluice outlet. Thus, deposition downstream extended upwards to the bed load sluice and the hopper. The upstream flow of the bed load sluice was also found to be disturbed by the mixing of the gravel flushing flow connected with the bed load sluice as depositions were observed upstream of the mixing point due to reduce velocities in this area.

Modifications adopted for the final arrangement

Following modifications were then adopted based on tests to eliminate the above mentioned factors that were identified to be problematic:

1. Crest height increased to 1.5 m to a length of 3.0 m , curved with a radius of 4m, starting with the trash removal section to increase the flushing head of the bed load sluice and create a stilling effect in the intake area decreasing sediment inflow to the intake.

Figure 73 Modifications at the intake of PHM of Khudi HPP (Shrestha et al., 2008)

The overall width of the hopper was reduced at its starting point, joined to the opening of the bed load sluice, by 3m with a side curve at the left bank.

The opening of the bed load sluice was reduced from the right most part to have a net opening of 1.45m, in order to increase suction and decrease sediment inflow into the bed load sluice. This helped to maintain the sediment load within the flushing capacity of the culvert downstream without flow pressurization. Furthermore, the gates were proportionally increased with an increase in the flow and operated as needed.

A new Intake flood wall was raised to an elevation of 947.00 masl adjusted at an angle with the initial flood wall end meeting tangentially to the curve wall at the left bank. A hood of one and a half meter width was introduced above the intake orifice top level to an elevation of the weir crest at 943.00 masl.

2. The gravel trap flushing canal was separated from the bed load sluice by setting it parallel to the bed load sluice canal and was also extended further downstream the bed load sluice to a length of 6.5m making an angle of 10 degrees to the river side with a slope of 1:50. The modification was meant to eliminate the flow disturbances due to mixing.

Figure 74 Modifications along the gravel trap on the PHM of Khudi HPP (Shrestha et al., 2008)

Similarly, the pressurized section of the gravel flushing canal was extended up to 3m downstream of it including the sharp bend in order to prevent flow separation in the bend section and increase its carrying capacity.

The top slab of the bed load culvert section was removed downstream the gate in order to avoid air pockets in the canal and supply air to ensure free flow in the channel.

3. The downstream river slope, shown in Figure 75, with boulder riprap, extending from the bed load sluice and the gravel trap was also maintained at 1:50 so that it could increase the efficiency of flushing. The modification also helped in preventing flow intervention downstream that would otherwise lead to deposition.

Figure 75 Modifications at the downstream river slope of Khudi HPP (Shrestha et al., 2008)

4. River training structures were introduced at the downstream if the flushing units at both banks as shown in Figure 76. River guide wall of about 15m was provided at the right bank downstream of the weir with a slope of 1:10 followed by a 32m long wall with a slope of 1:20 and a front face sloped at 6:1 (V:H). The gravel trap wall was extended by a few meters to a length of 9 m on the left bank and curved to meet the river topography.

Figure 76 River training structures Khudi model (Shrestha et al., 2008)

5. Sediment load reduction towards the intake was achieved by introducing a curve at the right bank upstream of the weir with a top elevation of 944.0 masl. A curve wall also provided at the left bank upstream of the weir axis with top elevation at 945.0 masl extending to the intake side wall. The curve provided an outer bend towards the intake reducing sediment load to the intake. A normal flow towards the intake was also secured to prevent the inflow of boulders during flood. The modifications are illustrated in Figure 77.

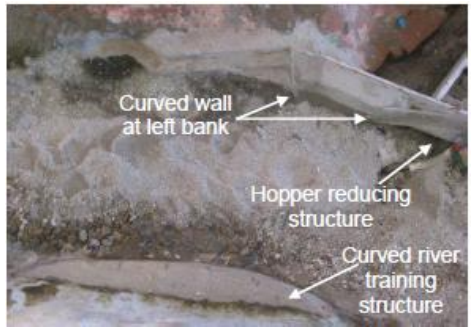

Figure 77 River training structures at the intake of PHM of Khudi HPP (Shrestha et al., 2008)

Effects and Evaluation of the modifications

Flow channelization downstream of the weir by separating the two flushing units to overcome the downstream deposition alone was found insufficient to increase the performance of the headworks. Increase in flushing head of the bed load sluice due to weir increment increased the stilling effect in front of the intake with an increased sediment diversion away from the intake and only movement of fine sediments towards the intake. The flushing capacity was immensely improved. However, turbulence was observed in front of the intake leading to increased flow trash and floating debris towards the intake.

Figure 78 Final arrangement of the PHM of Khudi HPP

Curved river guide walls and diagonal weir installed upstream of the weir axis helped decrease the sediment load towards the intake. The removal of the top slab of bed load culvert section downstream of the gate and reduction of the bed load opening aided in bed load flushing. The sediment concentration used in the model were realized to be much more than reality and in consultation

with the client and the design consultant the sediment load was reduced to one third of the concentration applied previously. The operation of the bed load sluice gate was proportionally increased with the flow as sediment load towards the intake increased with increase in the openings of the flushing unit. Similarly, the gravel flushing was operated as required. The adopted solutions were satisfactory for passage of sediments and sediment removal from the intake. Turbulence in front of the intake was still existent.

A wall was added downstream of the weir axis to obtain smooth flow downstream of the flushing units. Structures were installed in front of the intake in variable numbers and of different shapes; however, these only intensified the vortices in between them, and was proved unsatisfactory. Hood above the intake with varying length from half a meter to two was used to induce pressurization at the intake reducing velocity. This increased suction from the bed load sluice, however the turbulence remained. Hopper size was also reduced. This reduced sediment inflow to the intake and a continuous suction was observed in the hopper with less deposition at the bed load sluice suction area. Vortex was reduced to normal rotational flow with occasional formation of suction vortex.

Trashes and debris were accumulated near the intake area due to reduction in suction capacity of the vortex. Provision of the hood at the intake orifice top level and a new positioning of the flood wall helped to remove trashes and sediments more efficiently. Operation of the gravel trap had to be done with a minimum possible opening of the bed load sluice. As the increased flushing capability and sediment diversion lead to vortex formations at the intake creating problem with trash and debris passage; the final design (Figure 78) of the intake structure is a compromise between trash removal and bed load removal in the headworks.

Appendix B Salient features for the initial headworks design of LMM HPP

S.No.	Item	Description
1.	**Project Name**	
		Lower Manang Marsyandi Hydroelectric Project
2.	**Name of the river**	
		Marsyangdi River
3.	**Location**	
		Headworks in Tachai-Bagarchap VDC and Powerhouse in Dharapani VDC, Manang District
3.1	**Project Boundary**	
		Longitude Latitude 84°21'55"E 28°32'30"N 84°20'00" E 28°30'00"N
4.	**Type of scheme**	
		Run-of-the-River (ROR)
5.	**Hydrology at the intake**	
	Catchment area	1694 km^2
	100 year Flood (Q_{100})	1211 m^3/s
	1000 year Flood (Q_{1000})	1613 m^3/s
	Mean monthly flow	46 m^3/s
	Design discharge (33 percentile flow)	52 m^3/s
	Diversion flood (20 years dry season flood)	230 m^3/s
6.	**Diversion weir**	
	Type	Ogee shaped free overflow concrete weir
	Length of weir	45m
	Weir crest level	2094 masl
7.	**Undersluice**	
	Gate type/number	Two sluice openings with radial gates

	Size of gates	4.5m wide and 9m high radial gate on the weir side 4.5m wide and 6.5m high radial gate with 2.5m high flap gate on top on the intake side
8.	**Intake**	
	Type	Side
	Number and size	Four side intakes 8.15m wide and 4m high
9.	**Gravel trap**	
	Number	Two
	Size	9.5m long and 9.6m wide and 6.6 m deep from the normal operating level
	Gravel flushing culvert	78.5m and 50m long culverts 1.5m wide and 1.5m high
10.	**Settling basin**	
	Type	Surface settling basin
	Number	Four basin with one hopper in each basin
	Length	160 m
	Width	8.2m
	Height	8.3m at the start section, 10.3 m at the mid section and 12.3m at the end section including 2.85m deep hopper
	Invert slope	1:40
	Flushing	Conventional gravity flushing
	Flushing culvert size	2.5m wide and 2m deep
11.	**Power and energy output**	
	Gross head	323m
	Rated net head	311.1m
	Installed capacity	138.41 MW
	Gross Annual energy	675.54 GWh
	Net dry season energy	77.96 GWh
	Net wet season energy	568.04 GWh
	Net annual estimated energy after deducting outage	646.00 GWh

Appendix C Velocity distributions along various Cross-Sections (CS)

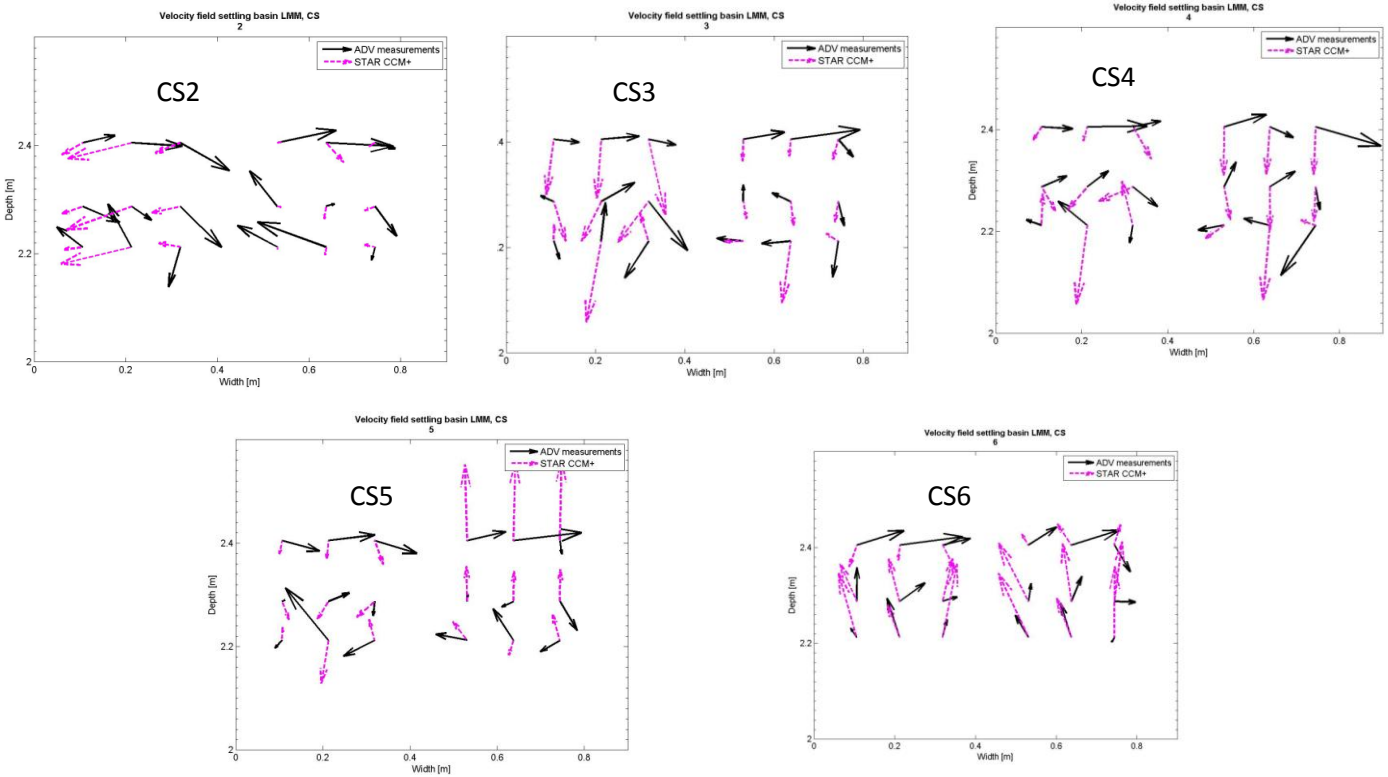

12 Appendix D Plan layout of the final design of LMM